Surface reactivity of anatase particles towards phosphated species

F. Guiot, C. Praud, S. Quillard, B. Humbert, M.-H. Ropers, M. Paris, H. Terrisse

Surface reactivity of anatase particles towards phosphated species

F. Guiot[a,1], C. Praud[a2], S. Quillard[a], B. Humbert[a], M.-H. Ropers[b], M. Paris[a], H. Terrisse[a,*]

[a] Nantes Université, CNRS, Institut des Matériaux de Nantes Jean Rouxel, IMN, F-44000 Nantes, France
[b] INRAE, UR1268 Biopolymères Interactions Assemblages, F-44300 Nantes, France

[*] Corresponding author.
IMN, 2 Rue de la Houssinière, BP 32229, F-44 322 Nantes, France
Tel: (33) 2 40 37 39 96
Email address: Helene.Terrisse@cnrs-imn.fr
ORCID: 0000-0002-9338-6939

Email addresses of other authors:
F. Guiot: florentine.guiot@univ-rennes1.fr
C. Praud: clement.praud@univ-nantes.fr
S. Quillard: Sophie.Quillard@univ-nantes.fr
B. Humbert: Bernard.Humbert@cnrs-imn.fr
M.-H. Ropers: marie-helene.ropers@inrae.fr
M. Paris: michael.paris@cnrs-imn.fr.

GRAPHICAL ABSTRACT

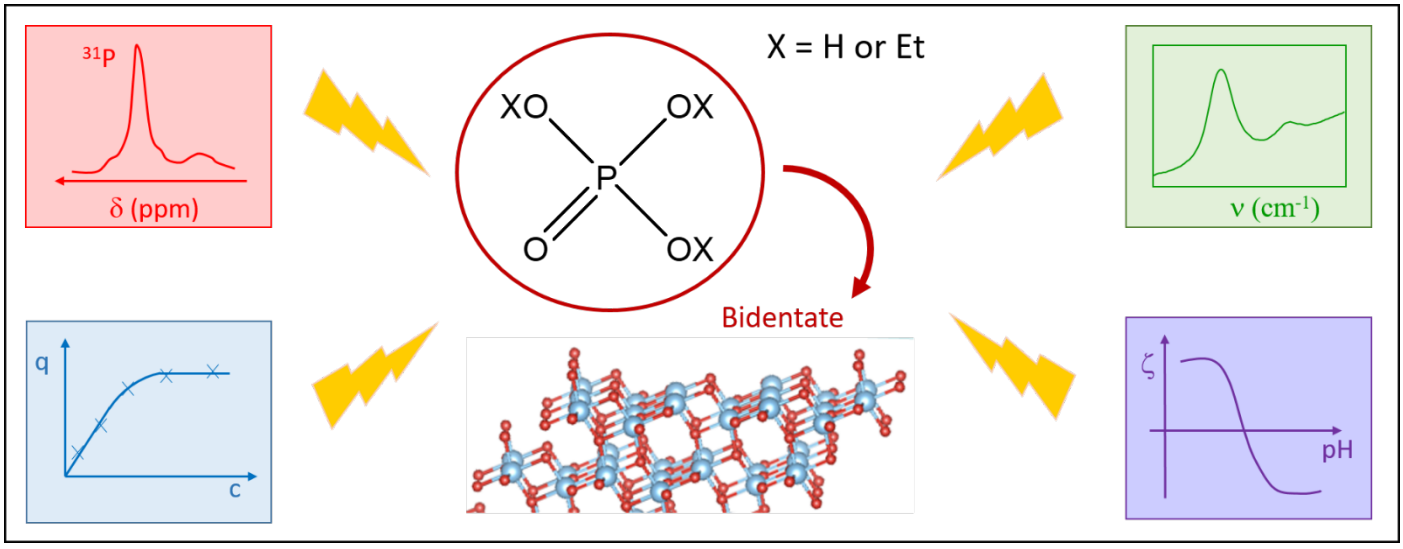

ABSTRACT

This multi-scale and multi-technique work investigates the adsorption of phosphated species on the TiO_2 anatase surface. Our original approach declines for the first time the progressive ethyl substitution of phosphates to identify the structure of complexes formed upon adsorption of these molecules on anatase in aqueous dispersions, under various pH conditions. To quantify the adsorbed amount of these molecules on

[1] Present address: Institut des Sciences Chimiques de Rennes (ISCR) - UMR CNRS 6226, 263 avenue du Général Leclerc, F-35042 Rennes, France.
[2] Present address: CEISAM UMR-CNRS 6230, 2 Rue de la Houssinière, BP 92208, F-44322 Nantes, France.

TiO_2, adsorption isotherms were recorded as a function of pH. In parallel, zeta potential measurements were performed to screen the evolution of the TiO_2 surface charge in the presence of the phosphated compounds. Lastly, surface complexes structure was characterized using spectroscopic methods: solid-state ^{31}P Nuclear Magnetic Resonance, Attenuated Total Reflectance Fourier Transform Infrared, and Diffuse Reflectance Infrared Fourier Transform Spectroscopy in the near infrared spectral range. Upon decreasing pH, the amount of adsorbed species increases, reaching a maximum of 1.5 phosphorus atom per nm^2 at pH 2. Monoethyl-phosphate remains adsorbed in similar amounts to orthophosphate, but di- and tri-ethyl substitutions lead to a sharp decrease of adsorption. Spectroscopic analyses reveal the affinity of othophosphate and monoethyl-phosphate for the anatase surface, with formation of bridging or chelating bidentate complexes, more or less protonated according to pH values.

KEYWORDS

TiO_2, anatase, phosphates, solid-liquid interface, adsorption, zeta potential, ^{31}P NMR, ATR-FTIR, Near Infrared, surface complexes.

INTRODUCTION

Titanium dioxide (TiO_2) is a metal oxide commonly used as a white pigment in various applications such as paints [1], cosmetics and food products [2]. In this last application, TiO_2 appears in the well-known food-grade additive named E171 in the Europe Union (EU) and INS171 in North America. This has been used for many years in the preparation of sweets, sauces, and cheeses for its coloring and brightening properties. Several studies [2-9] have revealed that a significant fraction of E171 particles are nanoparticles, and as a consequence, the question of their potential toxicity against living organisms was raised. Numerous studies have addressed the issue of hazards and risks caused by E171 [10-26], and among them, a work on the oral toxicity of E171 showed potential carcinogenesis-promoting effects in rats [12]. This finding recently led to the prohibition of titanium dioxide in food in EU[3]. However, due to their intensive use in industrial and personal care products, TiO_2 nanoparticles are released in large amount in the natural environment, especially aquatic, and they may have significant impact on environmental and public health, as highlighted in a recent review which pointed out the toxicological effects of titanium dioxide on exposed bivalve molluscs [27]. Moreover, use of titanium dioxide in food remains possible in the US and other countries, thus the question of its toxicity for human beings remains a current issue. Therefore, it appears that new studies should be conducted in order to explore the interactions between biological tissues (especially cell membranes) and titanium oxide nanoparticles. Fundamental studies have targeted the nature of the interactions involved between TiO_2 NPs and biological molecules present in cell membranes, such as phospholipids [28-40]. These studies suggest that the polar head group of phospholipids plays a major role in the binding with TiO_2 surface groups, which may be of a chemical nature [28, 37-39]. Moreover, various studies suggested that phosphate groups could form covalent bonds with the surface hydroxyl groups of TiO_2 [41-45]. However, literature data on this subject remains poor, and currently the binding modes of phosphates or phosphate-based molecules on the surface of titanium dioxide are not clearly identified. This information would be of great interest, not only in the context of food to evaluate the potential affinity of TiO_2 NPs towards cellular membranes, but also in the field of separation between lipids or peptides performed through columns filled with TiO_2 particles, which are able to specifically retain phosphated lipids or peptides thanks to their high affinity for these molecules [46-52].

[3] https://nanotech.lawbc.com/2022/01/ec-adopts-ban-on-use-of-titanium-dioxide-e171-as-a-food-additive/

In this study, through a multi-scale and multi-technique approach, we aim at investigating more precisely the nature of the interactions involved between phosphate head groups and TiO_2 surface. As E171 is mainly constituted of anatase crystallographic phase [4], we used a commercialized anatase powder (named PC100), chosen with a significantly high specific surface area, in order to enhance adsorption and thus to facilitate the quantification and spectroscopic characterization of adsorbed molecules. This TiO_2 powder was first characterized in terms of structure, morphology, particle size and specific surface area. Phospholipids being difficult to solubilize in water, we chose to work on small phosphated molecules, first to mimic the behavior of the head groups of phospholipids, and second to reach an extensive understanding of phosphate binding modes with the hydroxyl groups of the anatase surface. This second purpose could be achieved by progressively substituting protons of the phosphoric acid molecule by ethyl groups, which provides less anchoring possibilities for these molecules.

Adsorption isotherms were conducted for each phosphated molecule, and the quantification of adsorbed species was performed through UV-Visible absorption measurements, for various pH values. The as-obtained powders of TiO_2, covered with adsorbed phosphated molecules, were characterized by ^{31}P solid-state NMR and infrared spectroscopies, in order to elucidate the binding modes of phosphate groups on TiO_2. In addition, zeta potential measurements were performed to evaluate the modifications of surface charge through adsorption on the anatase surface, according to pH, which enables to get complementary information about the adsorption mechanisms involved.

This constitutes an original work, which combines spectroscopic features with macroscopic data to elucidate the binding modes of molecular species on an oxide surface, through a systematic investigation approach with close molecular structures, enabling a fine understanding of the involved mechanisms.

MATERIALS AND METHODS

TiO_2 sample

TiO_2-PC100 was purchased from Millennium Inorganic Chemicals. The powder was first washed in nitric acid 1 mol/L (1M) for one day. Then it was rinsed several times with deionized ultrapure Milli-Q water (Millipore, 18.2 MΩ.cm) and dried one week in a desiccator before use. This preliminary preparation ensures a clean surface before the adsorption of phosphated molecules. Infrared measurements confirmed the absence of nitrate species (expected around 1300 cm^{-1}) adsorbed on the TiO_2 surface (**Figure S1**).

X-ray diffraction (XRD, Bruker AXS D8 Advance, Bruker, Germany) data showed that the as-prepared PC100 is only composed of the anatase crystallographic phase of TiO_2 (**Figure S2**). The shape and size of PC100 particles were characterized using transmission electron microscopy (TEM, Hitachi H-9000 NAR (300 kV, Scherzer resolution 0.18 nm)). Most particles are ellipsoidal with an average size of around 20 nm. Some images also show some agglomerates of very small particles (below 5 nm), indicating that this commercial sample is not really homogeneous (**Figure S3**).

The specific surface area of the cleaned PC100 sample was evaluated to 76.8 ± 0.2 m^2/g, from the volumetric adsorption isotherms at 77 K of nitrogen gas followed by the Brunauer-Emmett-Teller (BET) adsorption treatment (Micromeritics TriStar II 3020 Physisorption Analyzer (Norcross, Georgia, U.S.A.)). Assuming that the nanoparticles are spherical, this method leads to a diameter of NPs close to 20 nm, in agreement with the images obtained by TEM.

Phosphated molecules

The Na_2HPO_4 (sodium hydrogenophosphate, Alfa Aesar, 99%) reagent was used to prepare phosphate solutions at various pH values. The monoethyl-phosphate compound was synthesized by following the method described by Dueymes et al. [53]. This synthesis leads to the cyclohexylammonium monoethyl-phosphate salt, where the cyclohexylammonium cation is the counter-ion of the once-deprotonated monoethyl-phosphate anion, and which was used directly. Diethyl phosphate (purchased as the 1-ethyl-3-methylimidazolium diethyl phosphate compound, > 98.0% purity) and triethyl phosphate (> 99.8% purity) were obtained from Sigma Aldrich and used without any further purification.

In the following, these compounds will be referred to as "P" for the non-substituted phosphate ion, and "MEP", "DEP" and "TEP" for the monoethyl, diethyl and triethyl substituted phosphates respectively (see **Figure 1**).

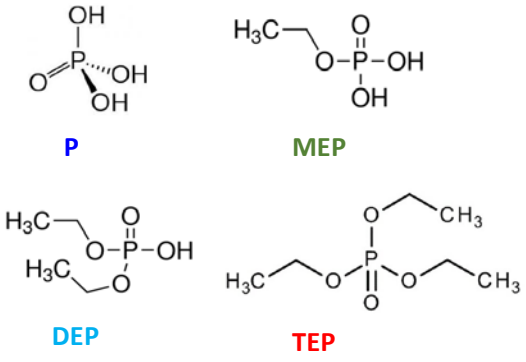

Figure 1: Chemical formulation of phosphated compounds used in the present study. "P" was purchased as the Na_2HPO_4 salt, "MEP" was synthesized under the $[CyNH_3](EtO)PO_3H$ compound (Cy = cyclohexyl; Et = ethyl), and "DEP" was purchased as the $[EMIM\text{-}(EtO)_2PO_2]$ salt (EMIM = 1-ethyl-3-methylimidazolium).

Adsorption isotherms protocol

PC100 aqueous suspensions (150 mg of solid for a liquid volume of 25 mL) were prepared in 50 mL plastic tubes for centrifugation. Sodium chloride (NaCl powder, Acros Organics, 99%), hydrochloric acid (HCl, 1M solution, Carlo Erba) and sodium hydroxide (NaOH pellets, Acros Organics) solutions were used to fix pH and ionic strength values of the suspensions. These suspensions were stirred at 25 rpm during 12h in the absence of light to hydrate the particles surface and then promote phosphated molecule fixation. Except for pH 2, the suspensions were prepared in a glove box (Plas-Labs, USA) under argon and with previously boiled ultrapure water (Millipore, 18.2 MΩ.cm) to avoid the presence of carbonates, known to adsorb on TiO_2 surface [54-58]. In the same time, a phosphated molecule stock solution (50 mmol/L) was prepared from P, MEP, DEP or TEP compound, in a volumetric flask of 25 mL (completed with an aqueous solution with the same fixed pH and ionic strength as the initial PC100 suspension). Increasing volumes of this stock solution were added to PC100 suspensions (from 100 to 1500 µL), then suspensions were completed to 40 mL by weighing, with a solution with fixed pH and ionic strength. Tubes were again stirred at 25 rpm during 24h in an oven (Memmert IPP500 108L, +5/+60°C) at 25°C. We verified that this duration was sufficient to reach equilibrium, confirming that no more variation of the phosphated molecules concentration in the solution could be observed. The pH of the suspensions was measured and adjusted to the set value all along this adsorption process. Then tubes were centrifuged a first time at 7800 rpm during 20 min. Supernatants were centrifuged a second time in the same conditions, while the solid was set in a desiccator under vacuum for 3 days to obtain dried powders. Once dried, solids were then analysed by IR and solid state ^{31}P NMR spectroscopies (see corresponding section). At the end of centrifugation, supernatants were filtered on microporous membranes with a pore mean diameter of 0.2 µm (Fisherbrand, syringe filters PES). This step could be insufficient to eliminate all particles in solution, thus in this case 50 to 200 mg of NaCl were added

in the supernatant before a second filtration. Increasing the ionic strength in solution leads to particle agglomeration, which facilitates filtration. In each case of fixed pH/ionic strength, a control sample was set up without phosphated molecules, which was used as a blank for IR measurements.

Supernatants were analysed by DLS (Dynamic Light Scattering, Zetasizer Nano-ZS, Malvern Instruments), in order to verify the lack of nanoparticles, and then the residual concentration of phosphated molecules was measured by UV-visible spectrophotometry (protocol described in the next section). Adsorption isotherms are plotted as the representation of the adsorbed phosphated molecules amount (reported in number of P atoms for one nm² area) according to the residual phosphated molecules molar concentration in the solution at equilibrium. For each condition of pH and ionic strength, a large panel of samples were prepared with various initial concentrations of phosphated molecules. Repeatability and reproducibility were checked with several experimenters. No error bars are indicated on the graphs since the estimation of uncertainty is quite complex for such measurements, given the number of steps. Instead, all experimental points are represented, in order to visualize the general tendency of these adsorption isotherms.

Dosage of phosphated molecules through UV-Visible spectrophotometry

For non-substituted phosphates (P)

First, a standard range was prepared with increasing phosphate concentrations in ultrapure water (from 50 to 2500 µmol/L). Then, in 15 mL plastic tubes for centrifugation, 40 µL of phosphate solution (either the supernatant to dose or the standard) were introduced with 600 µL of 1 mol/L hydrochloride acid, and the mixture was heated in a thermal bath (Memmert, 10L WNB10) at 90°C during 15 min. At last, 1.4 mL of a combined reactive, which was constituted of one volume of a L-ascorbic acid solution at 10% w/w (prepared from $C_6H_8O_6$ powder, Alfa Aesar) for six volumes of a tetrahydrate ammonium molybdate solution at 0.42% w/w in 0.5 mol/L sulphuric acid (prepared from $(NH_4)_6Mo_7O_{24}$ powder, Sigma Aldrich), was introduced and tubes were heated again at 70°C during 20 min. In these conditions, a blue complex formulated as $PMo_4^{V}Mo_8^{VI}O_{40}^{7-}$ formed in solution [59]. Spectrophotometric measurement of the 824 nm absorbance (Perkin Elmer spectrophotometer equipped of 3D WB Det module) was then performed to determine the residual phosphate amount in the supernatants, by external calibration with the prepared standard solutions. Ultrapure water was used as a reference for these measurements. The amount of adsorbed phosphates on the PC100 surface was calculated by subtracting the residual concentration in the supernatants from the initially introduced phosphate concentration, and the result was expressed in P/nm^2, taking into account the solid weight in the solution volume, as well as the specific surface area of PC100 sample.

For substituted phosphates (MEP, DEP, TEP)

A standard range was prepared for each molecule, with the MEP, DEP or TEP species respectively, at increasing concentrations (from 500 to 2500 µmol/L). There is one more step in this protocol than the previous one used for non-substituted phosphates. Indeed, the O – C bond between the ethyl groups and the phosphorus atom has to be broken, before the blue complex can be obtained. For this purpose, in a quartz tube (Technical Glass Products, USA), 40 µL of substituted phosphate solution (either the standard or the supernatant to dose) and 60 µL of a nitrate magnesium solution, prepared from $Mg(NO_3)_2.6H_2O$ powder (Sigma Aldrich, ≥ 99.0%), at 10% w/w dissolved in a solvent mixture composed of 95% absolute ethanol (Carlo Erba, ESR quality, 99.9%) and 5% ultrapure water, were introduced. Tubes were warmed with a torch (Castolin soldering lamp, ESC 768171) until orange vapours disappeared. Then, 600 µL of 1 mol/L hydrochloric acid were added after tubes have been cooled at room temperature. Tubes were then heated at 90°C in a thermal bath for 15 min. Lastly, 1.4 mL of the combined reactive was added (same composition as before), and tubes were heated again at 70 °C for 20 min. The rest of the protocol is similar to the previous one.

Zeta potential analyses

Suspensions constituted of around 5 mg of PC100 powder in 35 mL of aqueous solutions at fixed pH and ionic strength values, also containing a known concentration of one of the studied phosphated molecules, were prepared in a glove box under argon. After equilibrium, the zeta potential measurements of these suspensions were performed at 25°C with the Zetasizer Nano-ZS from Malvern Instruments. The analysis method relies on the electrophoretic mobility measurement at the shear plane and its conversion in a zeta potential value with the Smoluchowski model. Mean zeta potential values are obtained after 6 successive measurements on the same aliquot of each sample. The repeatability of the analyses was assessed on at least two different samples for each experimental condition. For each sample, pH was measured right before the zeta potential analysis, in order to get the best fit between the pH and the mean zeta value determined. The error bars indicated on the graphs correspond to uncertainty calculated from the zeta potential values resulting from the 6 successive measurements performed on the various samples (at least two) prepared in the same conditions.

Infrared absorption measurements

The infrared spectra, recorded by Attenuated Total Reflection (ATR) and Diffuse Reflectance Infrared Fourier Transform Spectroscopy (DRIFTS), were measured on a Bruker Vertex 70 spectrometer. For medium infrared range (MIR) we used an ATR accessory (Specac Quest ATR (single-reflection on monolithic diamond ATR crystal)). The Praying Mantis™ setup (Harrick Scientific Products Inc.) was used for the DRIFTS measurements, in the near infrared range (NIR). This system allows a highly efficient diffuse collection and minimizes the detection of the specular component. The powder sample was placed in an air purified sample compartment (CO_2/H_2O free). All the spectra were recorded at 4 cm^{-1} as spectral resolution and with 400 scans for DRIFTS and 100 scans for ATR (OPUS software 7.0). The reference subtraction from some ATR spectra was made with the OPUS software 7.0. The DRIFTS spectra were collected during 3h in the sample compartment, for an optimal dehydration of the samples (see **Figure S4**).

NMR spectroscopy

{^{1}H}-^{31}P CP-MAS (Cross-Polarization and Magic Angle Spinning) spectra were acquired on a Bruker spectrometer (11.7 T). The powders were introduced in a ZrO_2 rotor of 4 mm outer diameter. The contact time for CP was 0.5 ms and MAS speed was 10 kHz. ^{1}H spinal decoupling (60 kHz) was used during acquisition. ^{31}P spectra were referenced against H_3PO_4.

RESULTS AND DISCUSSION

1) Adsorption isotherms of phosphated molecules on PC100 anatase TiO_2 particles

a) Non-substituted phosphates: evolution versus pH for I = 0.01 mol/L

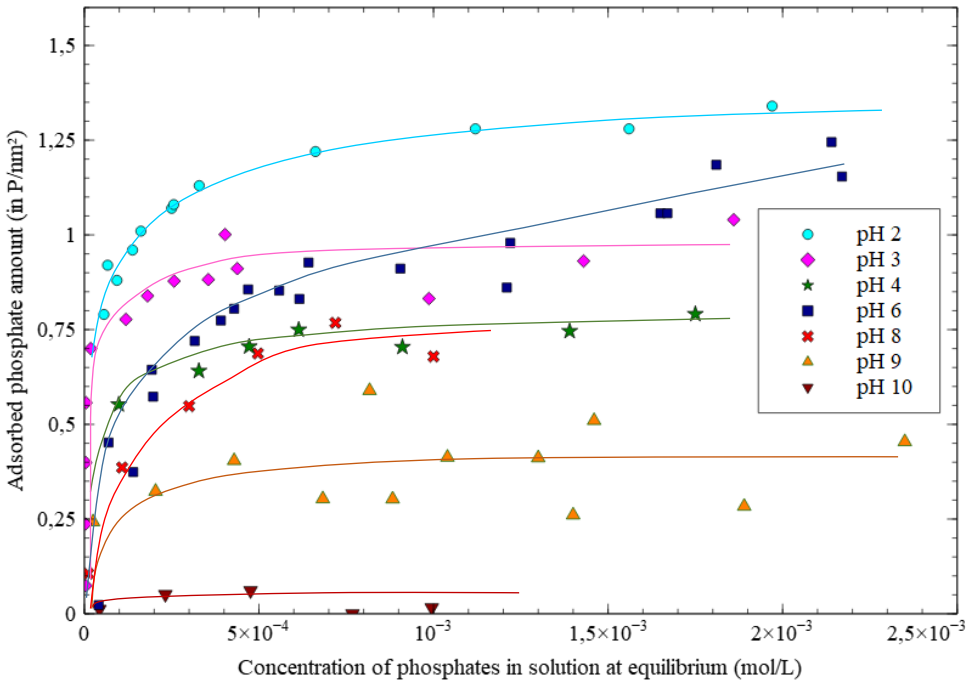

Figure 2: Adsorption isotherms of phosphates for different pH values at an ionic strength of 0.01 mol/L (fixed with NaCl salt), obtained at 25°C. These data were recorded with 11.5 m^2 of TiO_2 (150 mg of solid with a specific surface area of 76.8 m^2/g) in 40 mL of aqueous solution. The lines have been added as a guide for the eye.

Figure 2 shows the adsorption isotherms of phosphates (P) for pH 2, 3, 4, 6, 8, 9, and 10, with the same ionic strength (0.01 mol/L fixed with NaCl salt). All isotherms present an increase of the adsorbed amount for low concentrations in solution, followed by a more or less visible saturation "plateau", which depends on the pH value. The maximum adsorbed amount is obtained at pH 2, with a "plateau" corresponding approximately to 1.3 ion per nm^2 at the TiO_2 surface.

Globally, when pH increases, the amount of phosphate ions adsorbed on the surface decreases, reaching 0.4 ion per nm^2 for pH 9. At pH 10, almost no adsorption could be detected. This is due to the respective charges of the anatase surface and phosphate species in solution. Indeed, for pH lower than 6, the anatase surface is positively charged, as revealed by zeta potential measurements (see further corresponding section), whereas phosphate ions present negative charges (the first pK_a of phosphoric acid being 2.1). For pH upper than 6, the anatase surface becomes negatively charged, which repels phosphate ions from the surface. A particular behavior must be highlighted for pH 6, where the adsorbed amount exceeds that observed for pH 4, and even for pH 3 at high concentration in phosphates. Moreover, for this pH the adsorbed amount seems to increase continually, without reaching a maximum value even at high concentration. This may be related to the isoelectric point of anatase, located at pH 6, for which the solid surface is globally neutral. However, no further explanation could be brought to this particular behavior.

These results are in agreement with the study performed by Kang *et al*. [60] about the adsorption of phosphates on P25 particles (constituted of a mixture of 80% anatase and 20% rutile). Even if the maximum adsorbed

amount at pH 4 we obtained is a little below theirs (around 0.8 at pH 4 in our study against 1.2 P/nm^2 at pH 4.5 in the study of Kang *et al.*), for pH 9 the results are in total agreement between both works (maximum adsorbed amount around 0.3 P/nm^2). The small difference observed at low pH may be due to the crystalline phase of TiO_2, since we worked on pure anatase, contrary to Kang *et al.*

The adsorption of phosphates on the anatase surface is thus partly governed by electrostatic forces. However, a non-negligible amount of phosphate ions remains adsorbed on the anatase surface despite repulsive electrostatic interactions, as observed at pH 9, which is the sign of chemical adsorption.

b) Non-substituted phosphates: evolution versus ionic strength at pH 2

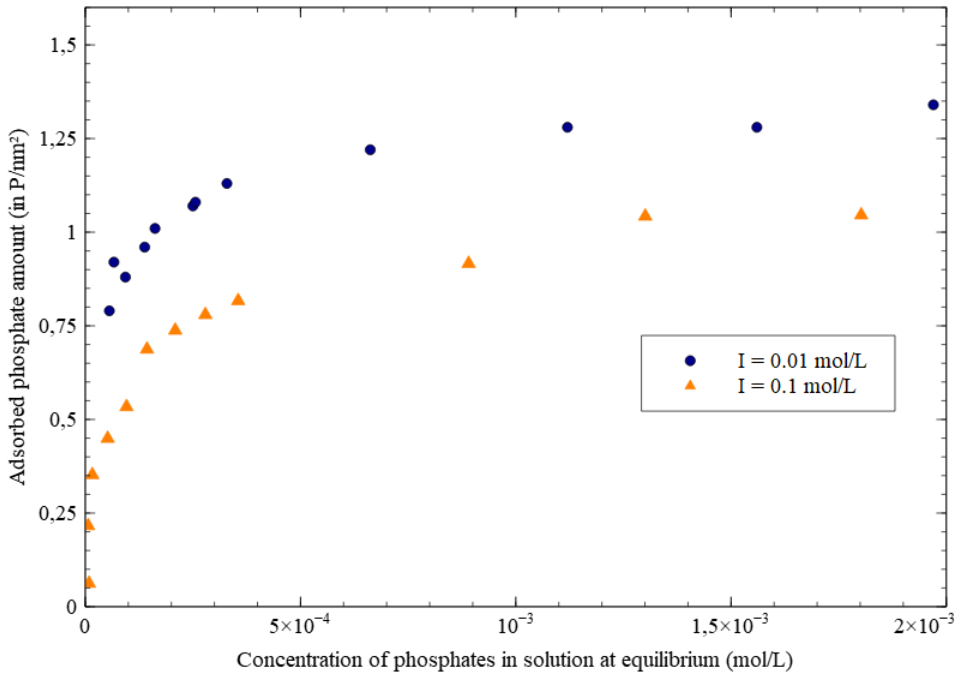

Figure 3: Adsorption isotherms of phosphates at pH 2 for two ionic strengths fixed with NaCl, 0.1 and 0.01 mol/L, at 25°C. These data were recorded with 11.5 m^2 of TiO_2 in 40 mL of aqueous solution. Data at an ionic strength of 0.01 mol/L correspond to Figure 2.

As seen in **Figure 3**, ionic strength significantly influences the amount of adsorbed phosphates for a fixed pH value, even if phosphate adsorption remains high after multiplying by ten the ionic strength (adsorption is reduced by around 20%). This behavior confirms that electrostatic forces are involved in the adsorption mechanism. Indeed, sodium and chloride ions screen the surface charge of anatase, lowering the attractive interactions with phosphate ions in acidic medium, which results in a decrease of the adsorbed amount. Hence, even if chemical adsorption is present, electrostatics could be significant in the adsorption mechanisms [61]. Physical bonding may thus also be involved in the interactions between phosphate species and the anatase surface.

c) Substituted phosphates: influence of pH and substitution on adsorption

Substitution on phosphate molecules modulates the adsorption. Adsorption isotherms of MEP on the PC100 surface could be established on the whole investigated pH range, similarly as P. For DEP, adsorption could be monitored only at pH 2. Indeed, at higher tested pH (6 and 9), adsorption of DEP could not be quantified on the TiO_2 surface: as the residual DEP concentration was very close to the initial introduced one, the difference was too low to be precisely measured. For the same reasons, no adsorption isotherms could be

achieved for TEP molecules, whatever the pH value. In these conditions, the results for MEP are presented at all pH values, while results for DEP are presented only at pH 2 and discussed at this pH with MEP and P.

Adsorption isotherms of MEP on PC100 obtained at pH 2, 4, 6 and 9, for an ionic strength of 0.01 mol/L (fixed with NaCl salt) are presented in **Figure 4**. The same tendency is observed as for P adsorption, with a global decrease of the adsorbed amount when pH increases (the maximum value drops from 1.5 molecule per nm^2 at pH 2 to 0.5 molecule per nm^2 at pH 9). At pH 2, the isotherm obtained with MEP does not present any well-defined saturation "plateau", contrary to that obtained with P. The maximum adsorbed amount (1.5 molecule per nm^2) is slightly higher than that observed for P in the same conditions (1.3 ion per nm^2). As a general trend, for each pH value the adsorbed amount of MEP seems to be a little larger than that of P (the difference varies between 5 and 25%).

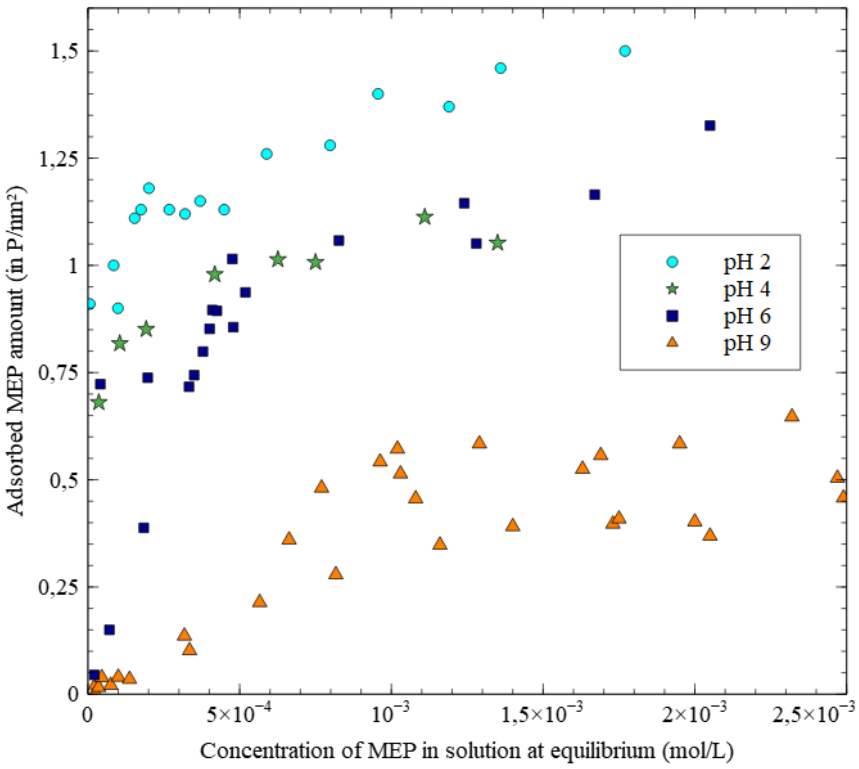

Figure 4: Adsorption isotherms of MEP for different pH values at an ionic strength of 0.01 mol/L (fixed with NaCl salt), at 25°C. These data were recorded with 11.5 m^2 of TiO_2 in 40 mL of aqueous solution.

For DEP (see **Figure 5**) at pH 2, the "plateau" corresponds to an adsorbed amount between 0.4 and 0.6 molecule per nm^2, which shows that this species is much less easily adsorbed on the TiO_2 surface than P and MEP, despite the low pH, which should promote the adsorption. Indeed, for this pH, the anatase surface is positively charged, whereas DEP is once deprotonated (pK_a = 1.39) and thus carries a negative charge.

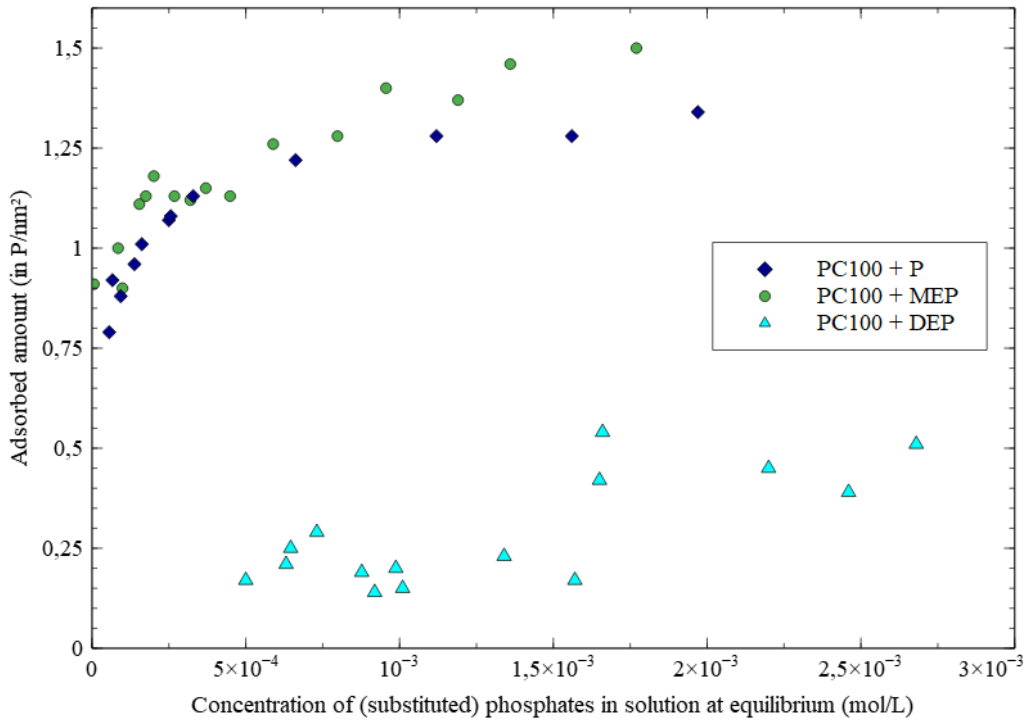

Figure 5: Adsorption isotherms of MEP, DEP and P at pH 2, for an ionic strength of 0.01 mol/L (fixed with NaCl salt) at 25°C. These data were recorded with 11.5 m^2 of TiO_2 in 40 mL of aqueous solution.

2) Zeta potential measurements

a) Influence of non-substituted phosphate adsorption on the zeta potential of anatase

Figure 6 shows the zeta potential evolution versus pH for PC100 samples, in a solution without phosphates, and in phosphate solutions at two different concentrations (2.5×10^{-6} and 1.0×10^{-5} mol/L). These low concentrations were chosen in order to reach almost total phosphate adsorption at the PC100 surface whatever the pH value, such as the phosphate concentrations in solution at equilibrium were negligible. The ionic strength was fixed at 0.01 mol/L with NaCl. The isoelectric point (IEP) of pristine PC100 sample is obtained for pH 6. When phosphate ions are present in solution, the IEP decreases, from pH 6 to pH 5 for a phosphate concentration of 2.5×10^{-6} mol/L, and to pH 4 for a concentration of 1.0×10^{-5} mol/L. This trend can be related both to the adsorbed phosphate amount and to the deprotonation of phosphate ions, according to pH. In acidic medium (pH 2), even if phosphates are adsorbed in large amount, they present a low negative charge, thus the zeta potential of anatase slightly decreases. When pH increases, the negative charge carried by phosphates raises, which leads to a significant decrease of the zeta potential (up to pH 6), since the adsorbed amount remains large in this pH range. Above pH 6, the adsorbed amount strongly decreases, however the negative charge carried by phosphates keeps growing, which can explain that the zeta potential remains more negative in the presence of adsorbed species than in their absence. This behavior was already evidenced in literature [62]: for a phosphate concentration of 1 mmol/L, the IEP of TiO_2 was found to shift down by 3 pH units. This IEP shift, as well as the charge reversal observed in the presence of phosphates, mean that strong specific adsorption of phosphate anions occurs on the TiO_2 surface: they are bonded to the solid surface through non-electrostatic interactions, probably forming inner-sphere complexes with the surface groups of TiO_2 [63, 64]. This result is in agreement with adsorption isotherms, which showed a significant amount of adsorbed phosphates at pH 9, even against repulsive forces. Moreover, the IEP value found for a phosphate concentration of 1.0×10^{-5} mol/L is in accordance with that obtained for E171 samples in our previous study [4], which was drastically lower than that of the P25 reference powder (80% anatase and 20% rutile mixture):

this behavior was explained by the presence of phosphate groups at the surface of the food additive (evidenced by XPS and IR characterization), which can be confirmed by the present study.

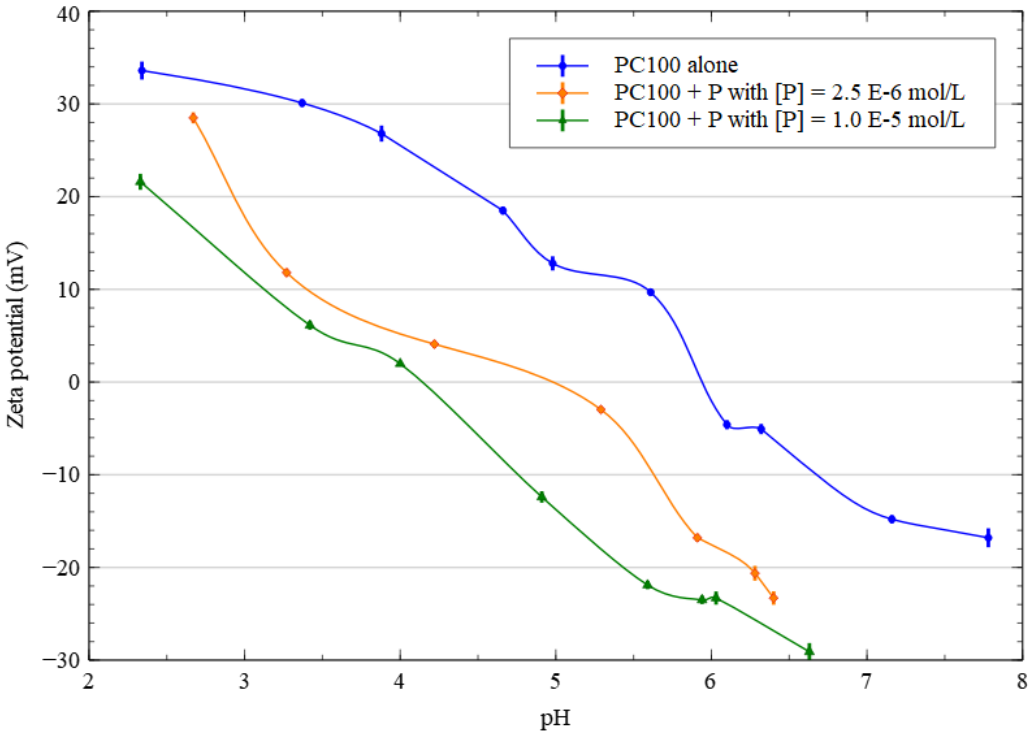

Figure 6: Evolution of zeta potential versus pH for PC100 in contact with phosphate ions at two concentrations 2.5 10^{-6} and 1.0 10^{-5} mol/L), compared with PC100 alone, at a constant ionic strength (0.01 mol/L fixed with NaCl salt). The solid concentration is 0.14 g/L.The lines have been added as a guide for the eye.

b) Zeta potential of anatase in the presence of various phosphated molecules

Figure 7 presents the zeta potential evolution versus pH for PC100 samples in contact with the various phosphated molecules, at the same concentration (1.0×10^{-5} mol/L), in comparison with pristine PC100, with a fixed ionic strength of 0.01 mol/L (NaCl). When the substitution of protons by ethyl groups on the phosphated molecules increases, the IEP, initially at pH 4 for P, tends towards that of pristine anatase (pH 6). This result firstly lies in the lower negative charge (coming from deprotonation of the hydroxyl groups) carried by the phosphated molecules when the number of ethyl groups increases (except for TEP, which is a neutral molecule), and secondly in the decrease of adsorbed amount when the number of ethyl groups increases, as shown by the adsorption isotherm results. In the case of MEP molecules, despite a similar adsorbed amount, the displacement of the anatase IEP is lower than for P ions, because of the smaller deprotonation ability of MEP compared to P, due to ethyl substitution. This IEP displacement in their presence suggests the formation of inner-sphere complexes with the TiO_2 surface [63, 64]. For DEP, although the IEP seems the same as that of pristine anatase, a less positive zeta potential is observed in acidic medium and a more negative one in basic medium, against repulsive forces, which reveals non-electrostatic interactions between these molecules and the anatase surface. However, the zeta potential evolution is very close to that of pristine PC100, given the low adsorbed amount of DEP molecules on the anatase surface, especially for pH higher than 6. Finally, TEP also seems to confer a more negative surface charge to anatase in basic medium, despite its neutral character, whereas for other pH values no significant modification of the zeta potential can be noticed compared to pristine anatase, in agreement with the negligible adsorbed amount for all the pH range.

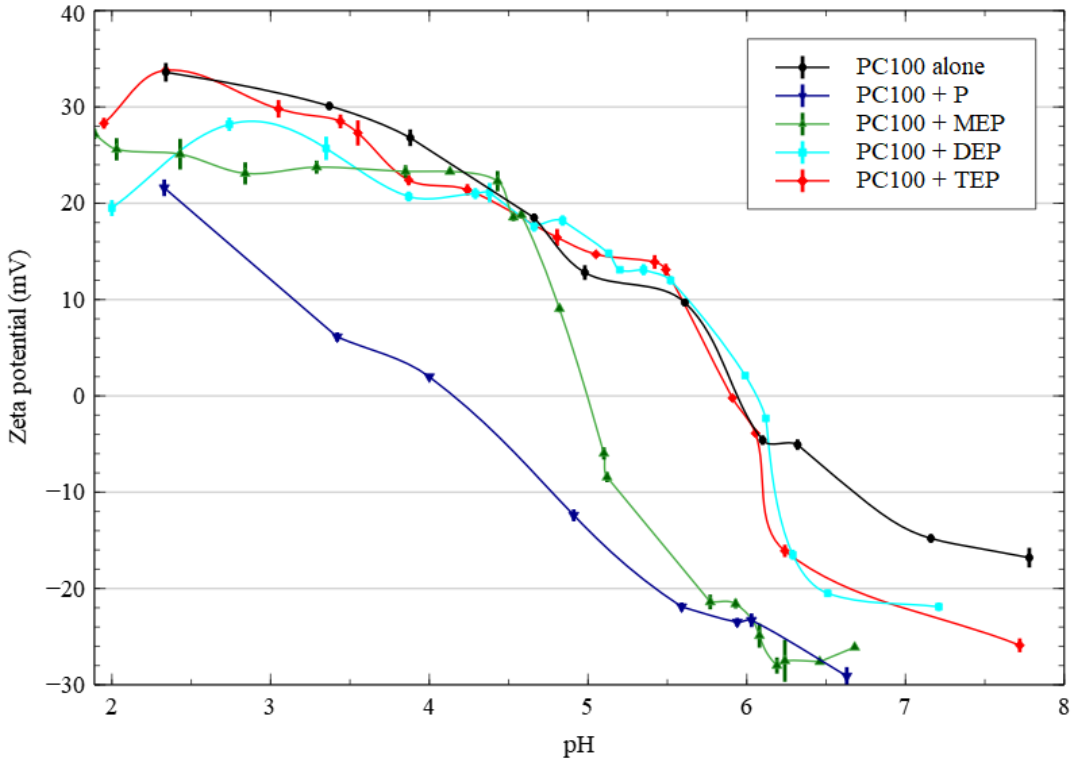

Figure 7: Comparative zeta potential versus pH evolution, for PC100 alone and in contact with phosphate ions (P) and substituted phosphate molecules (MEP, DEP, TEP) at the same concentration ([P] = 10^{-5} mol/L), with a constant ionic strength fixed with NaCl (0.01 mol/L). The solid concentration is 0.14 g/L. The lines have been added as a guide for the eye.

To briefly summarize these results, obtained on one hand through adsorption isotherms, and on the other hand by zeta potential measurements, they give macroscopic information about the phosphated species adsorption on the anatase surface: P ions and MEP molecules are adsorbed in significant amount on the solid surface, especially at low pH, which leads to a strong decrease of the anatase IEP. In contrast, DEP and TEP molecules are adsorbed in much lower amounts; thus they poorly disturb the solid-liquid interface, which leads to a very slight evolution of the zeta potential of anatase, with no displacement of the IEP.

3) Spectroscopic characterizations of phosphated molecules adsorption on PC100 anatase TiO_2 particles

For a fixed pH, the TiO_2 powders obtained through the adsorption isotherm protocol after drying of the solid phase, and for an adsorbed amount corresponding to the "plateau" of the adsorption isotherm, were characterized by ^{31}P solid-state NMR and infrared spectroscopies. These results provide information about the nature of the binding modes, considering the effects of the substitution degree and the pH values. These solid samples are referred to as P_{ads}, MEP_{ads}, DEP_{ads} and TEP_{ads} in this spectroscopic part.

a) Infrared measurements

Despite samples were dried before infrared analyses, a small fraction of water is still present at their surface, which leads to the presence of hydrogen bond network. The latter may vary the infrared transition moment, thus complicating quantitative analysis of the obtained results. Moreover, this hydrogen bond network is affected both by the ethyl substitution on phosphated compounds and by the pH. As a consequence, the results presented in this part will be mostly qualitative, or semi-quantitative for some of them.

- **Effect of substitution level**

In **Figure 8A** are presented the NIR-DRIFTS spectra of PC100 powders obtained after equilibration at pH 2, in aqueous solutions with an ionic strength of 0.01 mol/L (NaCl) and containing one of the four phosphated compounds (P, MEP, DEP and TEP). The broad absorption band at 2500-3500 cm^{-1} is due to the stretching of OH groups involved in hydrogen bonds, and the narrower bands between 3600-3800 cm^{-1} correspond especially to the TiO-H [65, 66] or PO-H [43, 67, 68] stretching, with weaker intermolecular interactions ("isolated" groups). The modes of PO-H group are clearly separated in the NIR range from the modes involving other O-H groups. Indeed, the combination modes give a much better possibility to observe infrared absorptions that are spectrally separated from the other absorptions than in the middle infrared, which only involves the fundamental modes. Thus, the band at 4663 cm^{-1}, assigned to the combination of stretching modes ($\nu_{P-O}+\nu_{O-H}$) of P-O-H [69-71], is the signature of adsorbed phosphated molecules on the TiO_2 surface, when possessing a P-O-H group.

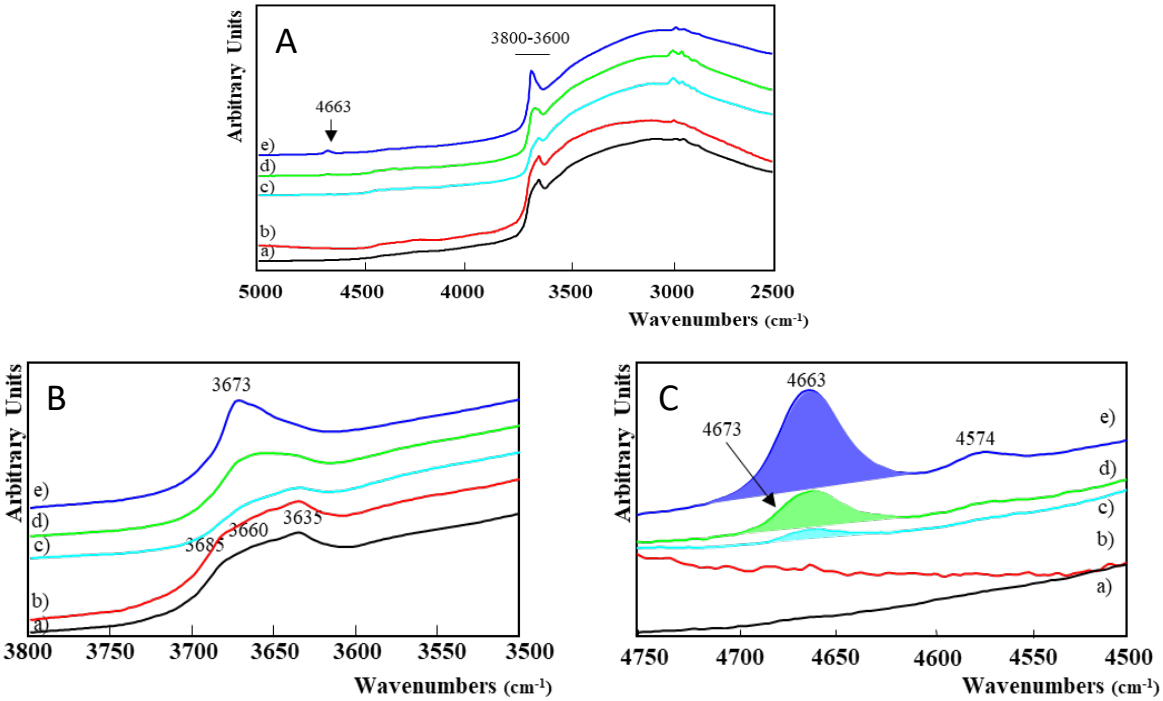

Figure 8: DRIFTS spectra of PC100 powder after adsorption of phosphated species, at pH 2 and with an ionic strength of 0.01 mol/L: A) 5000-2500 cm^{-1}; B) 3800-3500 cm^{-1}; C) Near infrared range, 4750-4500 cm^{-1}.
a) reference PC100; b) TEP_{ads}; c) DEP_{ads}; d) MEP_{ads}; e) P_{ads} (the spectra are offset for visibility, and the combination modes involving P-O-H are evidenced by band coloring).

These main features are more visible in **Figure 8B** and **Figure 8C** for the range 3500-3800 cm^{-1} and 4500-4750 cm^{-1} respectively. Three bands (at 3635, 3660 and 3685 cm^{-1}) are displayed in **Figure 8B** for the reference surface of PC100. These bands correspond to stretching modes of TiO-H in various environments, *i.e.* TiOH, $TiOH_2$ or Ti_2OH. On the basis of previous results [65, 66], the bands with lower frequency (< 3680 cm^{-1}) are assigned to bridging hydroxyl groups Ti_2-OH and the band at higher one (> 3680 cm^{-1}) to terminal hydroxyl groups Ti-OH or Ti-OH_2. On one hand, these three bands are still observed after adsorption of TEP (**Figure 8B**, spectrum b), confirming a very weak adsorption of these molecules on the anatase surface. On the other hand, the profile of this massif is considerably modified after adsorption of the other phosphated species (**Figure 8B**, spectra c, d and e). Both absorption signals at 3635 and 3660 cm^{-1} decrease drastically, moreover we can notice that one new component (around 3673 cm^{-1}) appears after adsorption of MEP, which is even more visible for P_{ads} sample. This component is associated to PO-H groups present at the surface [67].

Lastly, at the same time, the intensity of the band at 3685 cm^{-1} seems to decrease, when passing from TEP_{ads}, to DEP_{ads}, to MEP_{ads} and then to P_{ads} sample.

In **Figure 8C**, the 4663 cm^{-1} band, related specifically to surface P-O-H group (combination of $\nu_{P-O}+\nu_{O-H}$) is clearly displayed for P_{ads} and MEP_{ads} samples but very less intense for DEP_{ads}, and finally absent for TEP_{ads} as for the PC100 surface reference. These displayed spectra are obtained upon dehydration of the samples, at room temperature under a stream of air dry, for three hours inside the spectrometer chamber, in order to eliminate water molecules physically adsorbed at the interface. Thus, the elimination of the H-bond interactions between water and O-H groups allows us to clearly characterize the P-O-H groups (**Figure S4**). The bands at 4663 and 3673 cm^{-1} show parallel behavior.

The area of this component centered at 4663 cm^{-1} is directly related to the amount of the adsorbed phosphated molecules possessing a PO-H group: its value decreases from P_{ads} (0.5 a.u.) to MEP_{ads} (0.2 a.u.) then to DEP_{ads} (<<0.1 a.u.) powders, and is equal to zero for TEP_{ads} and for the reference. These values give only a tendency because the H-bond environment differs for P, MEP and DEP, and then disturbs the infrared transition moment. These results confirm that adsorption of phosphated species occurred in the case of P, MEP and DEP molecules. In the case of TEP, since no PO-H group is displayed on this compound, no information concerning a possible adsorption of this molecule on the anatase surface can be extracted from this peak. Let us notice that this band at 4663 cm^{-1} shows a shoulder at higher wavenumber (around 4673 cm^{-1}), especially for MEP_{ads} and DEP_{ads} samples. Another combination is also displayed in this wavenumber range, at a lower value around 4574 cm^{-1}, clearly visible for P_{ads} and MEP_{ads} samples.

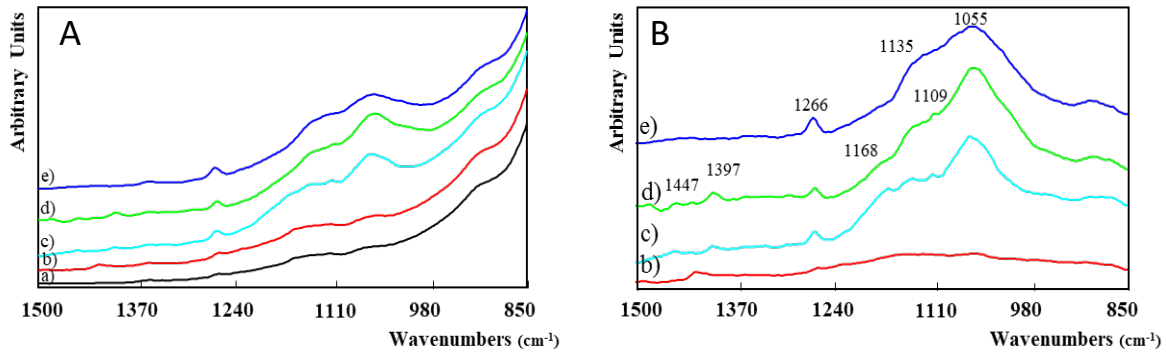

Figure 9: MIR-ATR spectra of PC100 after adsorption of phosphated molecules, at pH 2 and with an ionic strength of 0.01 mol/L: A) as-recorded spectra; B) spectra after subtraction of the PC100 surface reference. a) reference PC100; b) TEP_{ads}; c) DEP_{ads}; d) MEP_{ads}; e) P_{ads} (the spectra are offset for visibility; the as-recorded spectra are not labelled to avoid the perturbation coming from the strong absorption of TiO_2).

In **Figure 9A** are presented the ATR spectra in the 1500-850 cm^{-1} range where main differences are observed between the various studied samples. Under 850 cm^{-1}, the strong absorption due to TiO_2 anatase does not enable to see the lower modes of phosphate groups. Comparing to the spectrum of PC100, new bands appear for the P_{ads}, MEP_{ads} and DEP_{ads} samples, in the same wavenumber range, while the TEP_{ads} sample is very close to the reference.

Let us note that the MIR-ATR bands observed on all spectra correspond undoubtedly to adsorbed phosphate species, since their wavenumbers are different from those of phosphate ions in solution, whatever the pH, as already observed by Tejedor-Tejedor *et al.* [72]. Furthermore, these wavenumbers are comparable to those reported in several works about the adsorption of orthophosphates on titanium oxide [42, 43, 73-75] and on other metal oxides [63, 72, 76], where they have been attributed to overlapping P−O vibrations.

In order to distinguish the bands more clearly, the reference PC100 spectrum was subtracted from the other spectra (**Figure 9B**). Between 900 and 1200 cm^{-1}, P-O and P-O-C stretching vibrations are expected [77, 78]. A broad band is observed for P_{ads}, MEP_{ads} and DEP_{ads}, with several components pointed around 1055, 1135 cm^{-1} for P_{ads} and 1055, 1109, 1135, 1168 cm^{-1} for MEP_{ads} and DEP_{ads}. No significant IR absorption is displayed in this range for the TEP_{ads} sample, confirming that the adsorption of this molecule on PC100 might be very weak. The bands at 1447 and 1397 cm^{-1} are only observed for the MEP_{ads} and DEP_{ads} powders, and can be assigned to the ethyl groups (CH_2/CH_3 bending) [79, 80]. A band at 1266 cm^{-1}, present for P_{ads}, MEP_{ads} and DEP_{ads}, decreases in intensity from P to MEP and then to DEP. The assignment of this band can be related to a PO-H bending mode [72, 77, 81] or a P=O one [82].

- **Effect of pH**

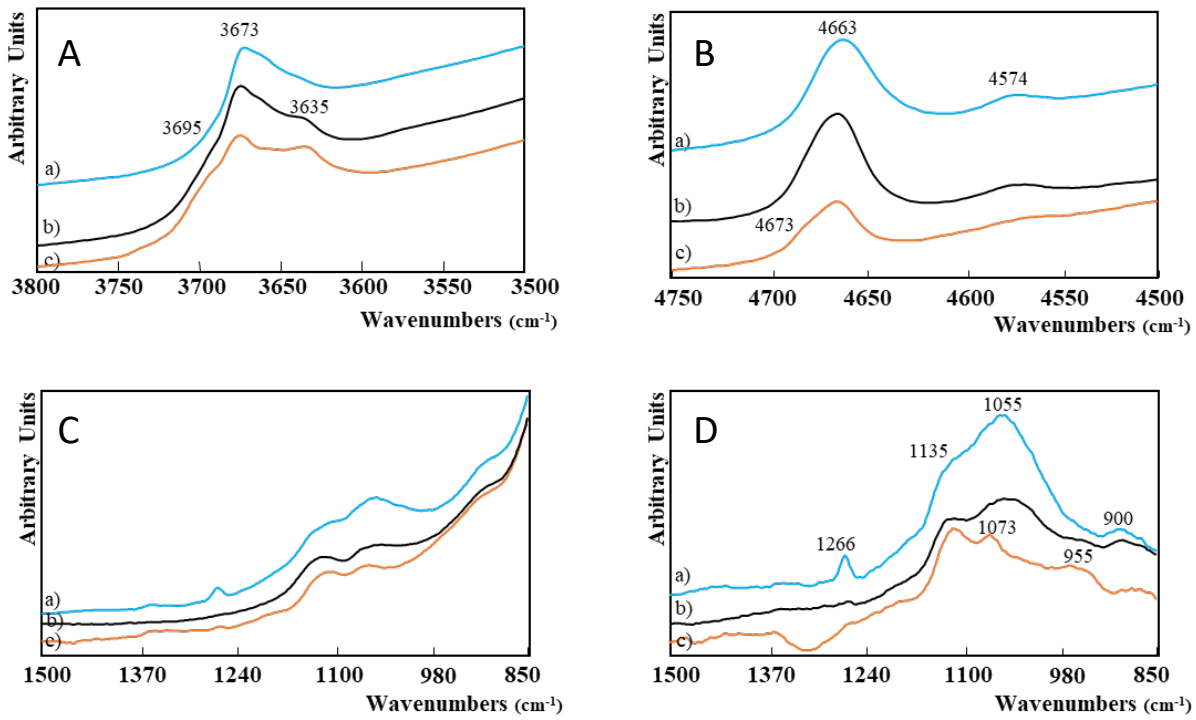

Figure 10: A and B) DRIFTS and C and D) MIR-ATR spectra of PC100 after adsorption of non-substituted phosphate ions with an ionic strength of 0.01 mol/L (C: as-recorded spectra, D: spectra after subtraction of the reference PC100 at the same pH).
a) pH 2, b) pH 6, c) pH 9 (the as-recorded spectra are not labelled to avoid the perturbation coming from the strong absorption of TiO_2).

The DRIFTS spectra obtained for P_{ads} samples at pH 2, pH 6 and pH 9 are presented on **Figure 10A and 10B**, with the same two frequency ranges as for pH 2 (see **Figure 8**). The P-O-H combination band at 4663 cm^{-1} is observed for P_{ads} at the three pH values, with a lower intensity at pH 9. The integrated areas for pH 2 and pH 9 are in a similar ratio as the maximum amounts of adsorbed phosphates in isotherms. The shoulder at 4673 cm^{-1} is more distinguishable as the pH increases. Concerning the MIR-ATR spectra (**Figure 10C and 10D)**, the bands related to the P-O stretching modes, expected in the 900-1200 cm^{-1} range, are much less intense for pH 6 and pH 9 than for pH 2. The main broad components are peaked at 1055 and 1135 cm^{-1} for pH 2 and pH 6, while at 1073 and 1120 cm^{-1} for pH 9. The band at 1266 cm^{-1}, observed for pH 2, is absent for pH 6 and pH 9. These results confirm that the phosphate adsorption decreases as the pH increases, as it has been shown via adsorption isotherm measurements.

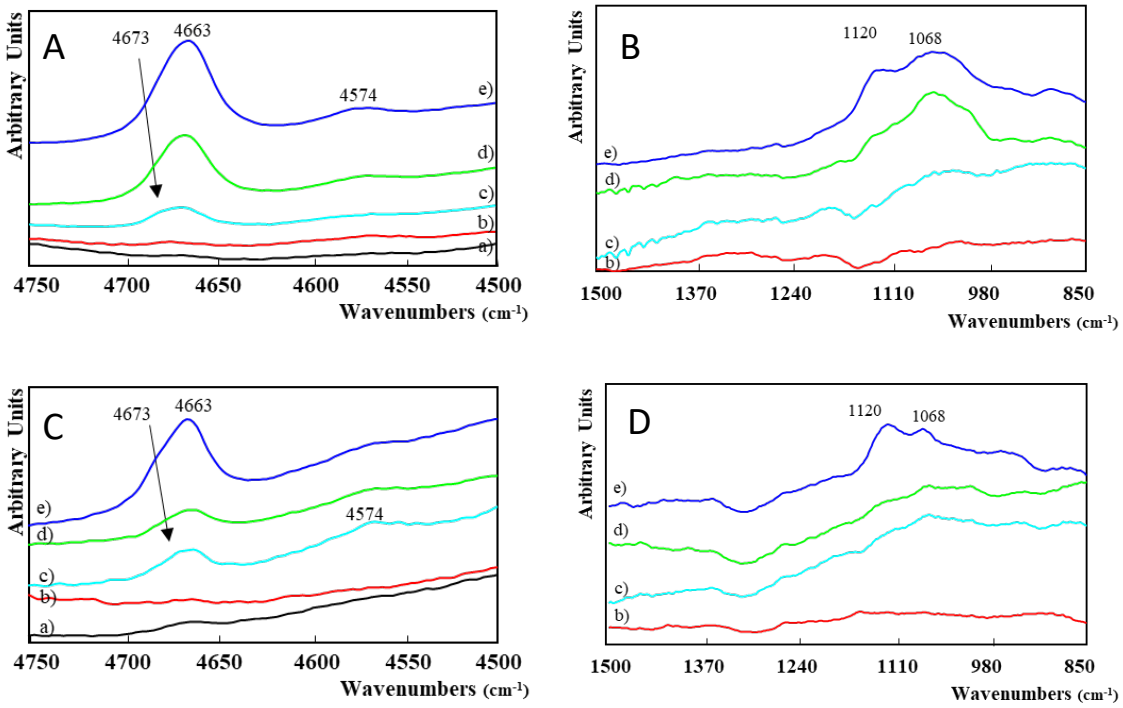

Figure 11: NIR-DRIFTS (4500-4750 cm^{-1}) and MIR-ATR (850-1500 cm^{-1}) spectra of PC100 after adsorption of phosphated molecules, with an ionic strength of 0.01 mol/L; A and B) pH 6; C and D) pH 9.
a) Reference PC100; b) TEP_{ads}; c) DEP_{ads}; d) MEP_{ads}; e) P_{ads}.

In **Figure 11** are reported the infrared spectra (NIR-DRIFTS and MIR-ATR) of TiO_2 samples covered with the different phosphated species at pH 6 (**A, B**) and pH 9 (**C, D**). These spectra confirm the decrease in the adsorbed amount as the pH increases for each phosphated molecule. For a fixed pH value, the intensities of the bands in the 900-1200 cm^{-1} range decrease (see **Figure 11 B, D**) as the degree of substitution increases. Thus, in agreement with the adsorption isotherms results, the phosphate adsorption decreases from P_{ads} to DEP_{ads} and is very low for TEP_{ads}. While P_{ads} and MEP_{ads} show similar MIR and NIR infrared profiles at pH 2 and pH 6, the P-O-H band at 4663 cm^{-1} is strongly less intense in MEP_{ads} than in P_{ads}. This feature partly reveals a similar binding mode for both compounds, with the presence of less P-OH groups in MEP_{ads}, as expected due to ethyl substitution in MEP molecules, but also maybe another different adsorption "complex". Moreover, at higher pH value (pH 9), MEP_{ads} spectra are closer to DEP_{ads} than to P_{ads} spectra.

b) Solid-state CP-MAS ^{31}P NMR measurements

- **Effect of substitution level**

The samples previously analyzed by infrared spectroscopy were also characterized by $\{^1H\}$-^{31}P CP-MAS NMR. This technique is not quantitative, as the resonance intensities depend on the polarization transfer efficiency between protons and phosphorus atoms, which can differ according to the chemical environment of each nucleus. However, relative intensities of each resonance can be compared between the various phosphated molecules adsorbed on the TiO_2 surface.

The spectra presented in **Figure 12** were recorded on PC100 samples in contact with the various phosphated molecules at pH 2. Except in the case of TEP_{ads}, several bands are clearly visible on these spectra, with at least 6 different chemical environments for phosphorus atoms. For each sample, the more intense band appears at

-3.4 ppm. The bands observed at 3.2, -3.4, and -9.1 ppm appear at exactly the same position for P_{ads}, MEP_{ads} and DEP_{ads} samples. However, their relative intensities differ notably, especially for the band at -9.1 ppm, which is largely more intense for MEP_{ads} and DEP_{ads} than for P_{ads}. This may be due to a better polarization transfer from ^{1}H nuclei, since MEP and DEP molecules present ethyl groups which can enhance cross-polarization compared to simple phosphate ions. Moreover, the bands at -1.3 and -6.4 ppm appear more clearly for DEP_{ads} sample, while for P_{ads} and MEP_{ads} ones the more intense band at -3.4 ppm only shows a slight asymmetry in both sides, suggesting the presence of the same bands as for DEP_{ads} but in lower proportions. For TEP_{ads} sample, the signal on noise ratio is very low in this range of chemical shifts (-10 to +5 ppm), and no resonance can be clearly distinguished, confirming the results obtained through infrared spectroscopy, showing very weak adsorption for TEP molecules. Hence, phosphorus atoms seem to present the same chemical environments, whatever the phosphated molecule except TEP, with similar bands located between 3.2 et -9.1 ppm, but the relative proportion of each environment differs from one molecule to the other. The last band observed on the spectra is rather large and located between -12.8 and -17.2 ppm (maximum at -15 ppm). This band presents the same form and position for P_{ads} and MEP_{ads}, while for DEP_{ads} it appears narrower and more intense, with a lower chemical shift (maximum at – 17 ppm). For TEP_{ads}, it is the only band of the spectrum getting out from the background noise, and it presents a similar chemical shift as P_{ads} and MEP_{ads}, with a just slightly greater intensity.

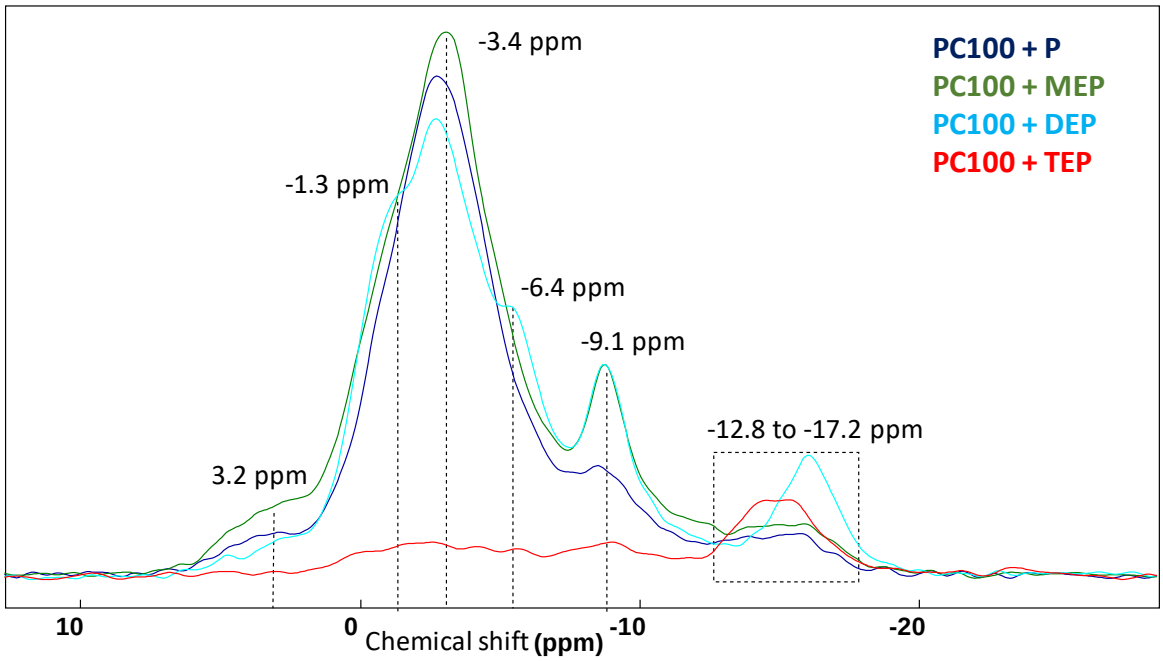

Figure 12: $\{^{1}H\}$-^{31}P CP-MAS NMR spectra of PC100 after adsorption of phosphated molecules, at pH 2 and with an ionic strength of 0.01 mol/L.

The results obtained on phosphate anions adsorbed on TiO_2 are similar to those presented by Kang *et al*. [60], with bands located in the same range of chemical shifts (they observed four peaks at 1.0, -2.4, -8.3 and -15.0 ppm).

- **Effect of pH**

As seen in **Figure 13**, where the CP-MAS NMR spectra of PC100 after adsorption of phosphate ions at three different pH values are presented, a decrease of the global spectrum intensity is observed when the pH increases, related to the lower adsorbed amount evidenced by isotherms. Moreover, there is a chemical shift evolution of the main band (centered on -3.4 ppm at pH 2) towards higher values (close to 0 ppm at pH 9). Kang *et al*. already noted this chemical shift evolution, which could be explained by changes in surface charge

and hydrogen bonding environment [60]. The band at -9.1 ppm seems to remain at the same position when the pH increases, while the large band between -12.8 and -17.2 ppm tends to vanish.

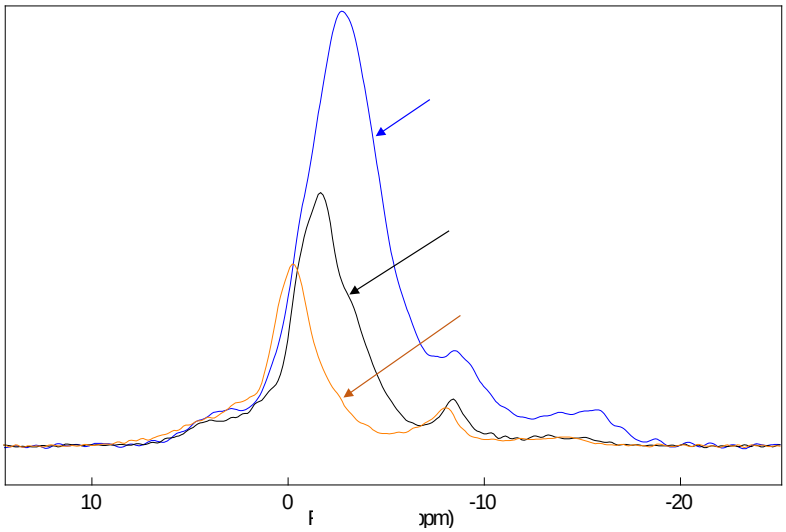

Figure 13: {^{1}H}-^{31}P CP-MAS NMR spectra of PC100 after adsorption of phosphate ions, for various pH values (2, 6 and 9), with an ionic strength of 0.01 mol/L.

When comparing the CP-MAS NMR spectra of various phosphated molecules adsorbed on PC100 at pH 6 (**Figure 14A**), it appears that the same bands are detected for P_{ads}, MEP_{ads} and DEP_{ads}, such as pH 2, whereas TEP_{ads} gives a very poor signal. The intensity of the main band, centered around -2 ppm, decreases when ethyl substitution increases in phosphated molecules. In contrast, for the three samples (P_{ads}, MEP_{ads} and DEP_{ads}), the intensity of the band at -8 ppm decreases less than that of the band at -2 ppm. The large band observed at pH 2 with a lower chemical shift (between -13 and -17 ppm) seems to be present with a very weak intensity on the spectra recorded at pH 6. However, increasing the acquisition time allows this band rising from the background noise (see **Figure S5** for DEP_{ads} and TEP_{ads} samples).

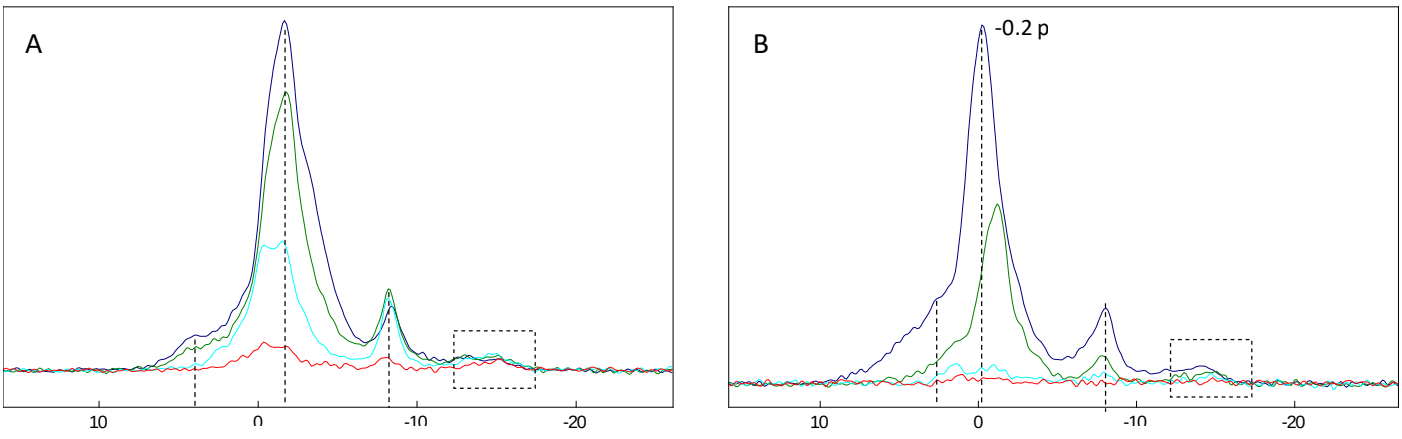

Figure 14: {^{1}H}-^{31}P CP-MAS NMR spectra of PC100 after adsorption of phosphated molecules at pH 6 (A) and pH 9 (B), for an ionic strength of 0.01 mol/L.

At last, at pH 9 (**Figure 14B**) DEP_{ads} and TEP_{ads} give almost no NMR signal, in agreement with the impossibility to quantify any adsorbed amount through adsorption isotherms. For P_{ads} and MEP_{ads}, similar

bands are observed, with very close chemical shifts. As for the other pH values, it suggests that P and MEP present similar phosphorus chemical environments, once adsorbed on the anatase surface.

4) Discussion about the binding modes of phosphated molecules on the anatase surface

At the beginning of this discussion, it seems important to underline that spectroscopic characterizations were performed on powders which were extracted from their equilibrium aqueous medium, and then dried. In these conditions, the adsorbed phosphated species remain anchored on the anatase surface, but their environment may have changed from their initial one, when the solid was in equilibrium with the aqueous phase. Nevertheless, these spectroscopic characterizations should give relevant information about the nature of surface complexes formed upon adsorption, even if the protonation state can differ from that of the hydrated solid.

Furthermore, we verified whether phosphate ions desorption was possible or not, by washing the obtained P_{ads} powders by aqueous solutions at the same pH and ionic strength (results not shown): these experiments let us know that adsorption was mainly irreversible, since a large amount of phosphates (between 80 and 85% at pH 2) remained adsorbed after washing. Moreover, NMR data showed that the remaining adsorbed phosphates presented the same chemical environments as before, the unique difference lying in a slightly lower relative intensity of the main band centered at -3.4 ppm at pH 2, indicating that this large band probably includes physisorbed species. The shoulder at 4673 cm^{-1} of the P-O-H combination band observed in NIR-DRIFTS measurements (**Figure 10**) may be associated to these species. Indeed, the shift of this band towards lower wavenumbers was observed after phosphate desorption.

Table 1 summarizes the main features of adsorbed phosphated molecules at the anatase surface, extracted from all characterizations previously described, and gives information about attributions of the IR and ^{31}P NMR bands, which are discussed in this section.

Table 1: Main characteristics of phosphated molecules adsorption at the PC100 anatase surface, including maximum adsorbed amount at three pH values, IEP of PC100 in the presence of phosphated molecules for [P] = 10^{-5} mol/L, main infrared bands with their qualitative intensities and their attributions, estimated relative adsorbed amounts at pH 2 extracted from IR spectra, and ^{31}P NMR chemical shifts with their proposed assignment. IR and NMR data are only given at pH 2, where the adsorbed amount reaches its maximum for each phosphated molecule. Band intensity is categorized as (+) low, (++) medium and (+++) high.

Adsorbed molecules	**P**	**MEP**	**DEP**	**TEP**
Maximum adsorbed amount (I = 0.01 mol/L)	• pH 2 → 1.34 P/nm^2 • pH 6 → 1.15 P/nm^2 • pH 9 → 0.45 P/nm^2	• pH 2 → 1.50 P/nm^2 • pH 6 → 1.33 P/nm^2 • pH 9 → 0.60 P/nm^2	• pH 2 → 0.54 P/nm^2 • pH 6 → non detected • pH 9 → non detected	• pH 2 → non detected • pH 6 → non detected • pH 9 → non detected
IEP of PC100 for [P] = 10^{-5} mol/L	pH 4.2	pH 5.1	pH 6.2	pH 5.9
IR bands (at pH 2) • 4663 and 3673 cm^{-1} → P-O-H • 1266 cm^{-1} → P-OH or P=O • 1055 and 1135 cm^{-1} → P-O • 1397 and 1447 cm^{-1} → CH_2/CH_3	+++ ++ +++ /	++ + +++ ++	+ + + +	No characteristic bands observed
Relative adsorbed semi-quantitative amount from IR (at pH 2)*	1.0	1.1	0.1	0.0
^{31}P NMR chemical shifts (at pH 2)	• From -9 to 3 ppm (several contributions) → bidentate (+++), possibly monodentate and physisorption • -15 ppm → monodentate (+)	• From -9 to 3 ppm (several contributions) → bidentate (+++), possibly monodentate and physisorption • -15 ppm → monodentate (+)	• From -9 to 3 ppm (several contributions) → bidentate (++), possibly monodentate and physisorption • -17 ppm → monodentate (++)	• -15 ppm → monodentate (+)

* Calculated from IR absorptions (DRIFTS and ATR spectra), and normalized on the amount of adsorbed P compound.

a) Discussion about the different binding modes, through NMR and IR results

NMR experiments on the various phosphated molecules can help identifying their binding mode on the TiO_2 surface. Indeed, DEP molecules cannot form tridentate complexes with the surface groups, due to their structure. Since the bands observed on the NMR spectra of DEP adsorbed on PC100 particles are similar as those present on the NMR spectra of adsorbed P and MEP, which could form tridentate species, we can eliminate this binding mode. This result seems in contradiction with those of Tielens *et al.*, who determined through calculations a good thermodynamic stability of tridentate complexes on the anatase (101) face [83]. However, their simulations show that this tridentate structure seems to be less favorable that monodentate and bidentate ones, and that its occurrence depends both on the exposed crystalline face and the work temperature.

Thus, our results support the very low probability for phosphates to form three Ti-O-P bonds with the anatase surface in aqueous suspension. Moreover, for TEP at pH 2, the large band between -12.8 and -17.2 ppm dominates the NMR spectrum. The unique possibility for TEP to adsorb on the anatase surface is through the formation of monodentate species, by the P=O double bond (maybe owing to hydrogen bonds). Hence, we may assign this large band at low chemical shift to monodentate binding on the TiO_2 surface. This large band at low chemical shift is also particularly intense in the case of DEP, for which the probability to form monodentate complexes is higher than for P and MEP, due to its only one P-OH bond free for anchoring to the anatase surface. Some authors also observed a large band between -15 and -20 ppm, and suggested that it could arise from minor phosphate polymerization on the anatase surface, due to solution concentration upon drying [83]. This hypothesis cannot be excluded in our study for phosphate ions, but a polymerization of TEP molecules seems to be less likely.

Consequently, we can suppose that the other bands appearing from 3.2 to -9.1 ppm mainly correspond to bidentate complexes, either by release of two protons of the hydroxyl groups (bridging complexes), or by release of only one proton, and thus involving delocalization of electrons between one deprotonated hydroxyl group and the P=O double-bond (chelate complexes). However, as they are also slightly visible for adsorbed TEP, especially at pH 6, it can be suggested that these bands, which are not really symmetrical, can contain a monodentate contribution (but probably less favorable than the bidentate anchoring), or may be partly assigned to physisorption through hydrogen bonding (which could explain the decrease of the intensity of this band after washing the powder). Thus, these conclusions suggest that P, MEP and DEP compounds may form in majority bidentate complexes on the anatase surface, in addition to monodentate ones which seem to be less favorable. This conclusion is in agreement with a recent computational work [84], where the authors observed a better stability of bidentate complexes than monodentate ones in the case of phosphate anions adsorbed on the (101) anatase surface, through adsorption energy considerations. **Figure 15** presents our propositions of binding modes for the various phosphated molecules, on the basis of spectroscopic results and literature data [41, 42, 83, 85]. For all structures containing one or more hydroxyl groups, the latter may be more or less deprotonated when pH increases.

Very few studies are reported on the interaction of phosphated compounds with titanium oxide using infrared spectroscopy, and they were mainly performed via *in situ* ATR measurements, which is different from our setup. Several authors mentioned that bidentate complexes should be the most probable species for orthophosphates adsorbed on TiO_2 [41, 42, 74, 75], especially for P and MEP compounds, which is in agreement with the previous conclusions we deducted from NMR results. Indeed, the main bands we observed at 1055 cm^{-1} and 1135 cm^{-1} (for pH 2), related to P-O stretching, are in good agreement with proposed bidentate assignment in literature data. IR spectra show that these bidentate species are more protonated at low pH, through the presence of the combination mode of $\nu_{P-O}+\nu_{O-H}$ at 4663 cm^{-1}. This P-O-H bond is more intense for P than for MEP, at pH 2 and pH 6 (see **Figure 11**), in agreement with the number of P-OH bonds of each compound. Moreover, the fact that the amount of hydroxyl groups attached to the phosphorus atoms is approximately double, considering the surface of this peak in IR spectra, for the adsorbed P species compared to the MEP species (0.5 versus 0.2 a.u.), goes qualitatively in the direction of a chelating bidentate structure of the adsorbed phosphate species, since for P the bidentate species exhibits two OH versus only one for MEP (see **Figure 15**). Thus, these IR results are consistent with the NMR conclusions concerning the preferential formation of bidentate complexes. The presence of the P-O-H combination band in the case of DEP confirms that monodentate binding is viable for this molecule, in agreement with NMR deductions (and in contradiction with previous results of Connor *et al*. [41]). Besides, the band at 4574 cm^{-1} (**Figure 10**) may also be related to monodentate anchoring: even if it is visible for all samples, its proportion relatively to the band at 4663 cm^{-1} is especially great for DEP. At high pH, the presence of the P-O-H combination band seems to indicate that a protonation is still possible, which may be surprising since P, MEP and DEP molecules should deprotonate for pH higher than their pK_a. As said previously, the powders with adsorbed phosphated

compounds are extracted from the aqueous medium. Moreover, IR recording is performed through air pumping during at least three hours, in order to eliminate adsorbed water which gives rise to IR bands overlapping with those of interest. This dehydration of the samples may disturb interface equilibrium, forcing the oxygen of adsorbed molecules to protonate back thanks to co-adsorbed water molecules or Ti-OH local groups. Hence, the P-OH bonds observed on IR spectra may not be representative of the protonation state in solution at the studied pH. However, IR gives a real image of the bonds involved in the molecules binding at the TiO_2 surface, and preserves information relative to the pH, such as the amount of adsorbed species. Nevertheless, dehydration of the samples may potentially force the bidentate complexes formation on the anatase surface.

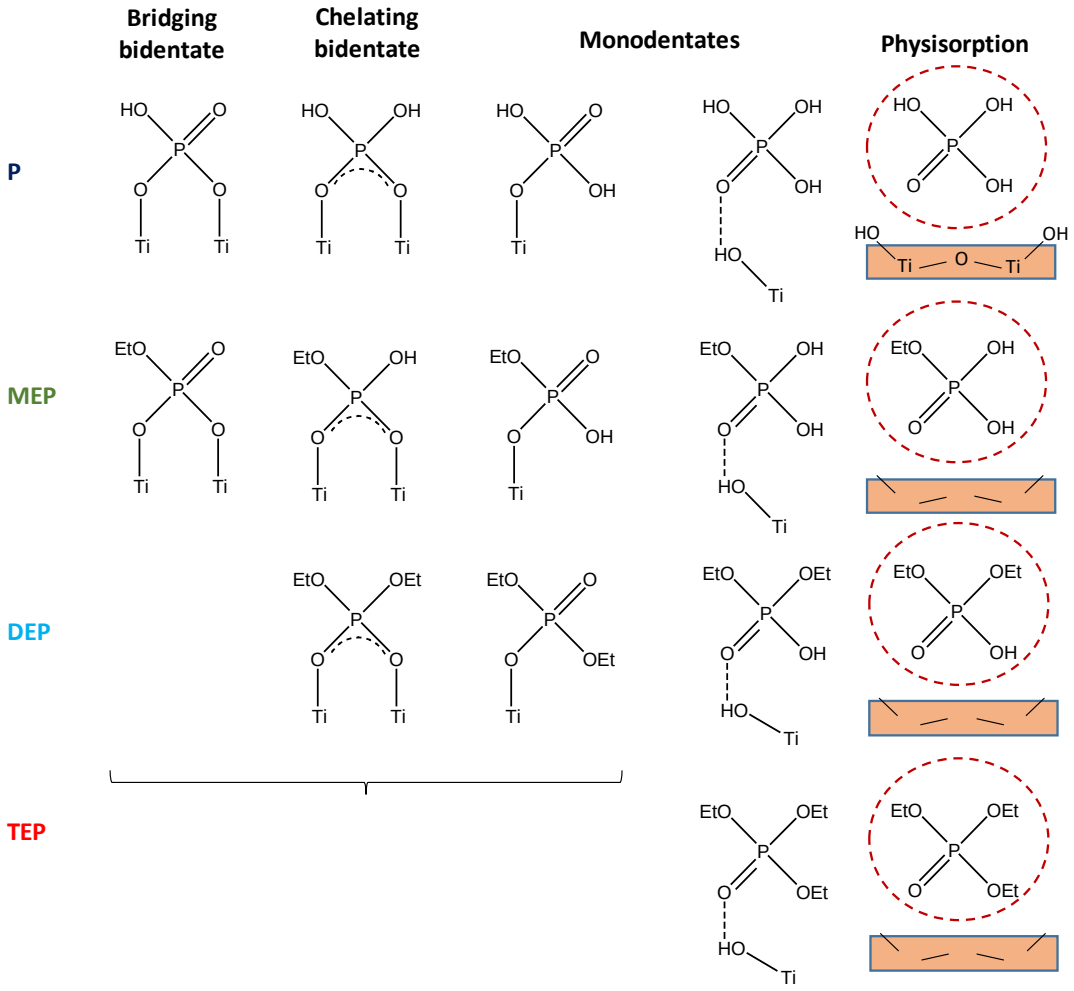

Figure 15: Propositions of binding modes for the various phosphated molecules on anatase surface. For simplification, water molecules are not included in these schemes.

b) Impact of MEP versus P on the zeta potential of anatase

Adsorption isotherms and spectroscopic measurements showed a similar behavior for P and MEP compounds, with comparable adsorbed amounts and same chemical environments in NMR spectra. However, the zeta potential analyses revealed great differences of surface charge between anatase particles in the presence of P and MEP, especially at low pH, below the IEP of TiO_2. This could be due to the difference of counter ion for both compounds: Na^+ for P ions, and cyclohexylammonium for MEP. The latter is larger than sodium ion and could bring a more positive charge at the solid-liquid interface, by laying inside the compact part of the electrical double layer. This could explain the more positive zeta potential in the presence of MEP for pH below 6, than for P in the same pH range. Another explanation could rely on the partly hydrophobic character

of MEP molecules, through their ethyl group, which may modify the dielectric properties of the solid-liquid interface. On one hand, MEP molecules would be more strongly bound to the surface than phosphates, and on the other hand, the ionic pair formed by the MEP anion and its cyclohexylammonium cation would be less dissociated.

c) Comparison of the ^{31}P chemical shifts for the various binding modes with literature data

A study performed in 1994 [86] assigned the ^{31}P NMR bands observed in bulk titanium phosphates to the connectivity of phosphorus tetrahedra with titanium atoms, and suggested that the ^{31}P chemical shift decreased from -5 ppm to -22 ppm when the number of titanium atoms binding the phosphorus center increased between 1 and 3. This implies that, in bulk titanium phosphate compounds, tridentate species would have a lower chemical shift than bidentate one, and that monodentate species would present the highest chemical shift. Lots of more recent studies on titanium phosphates based their assignment of ^{31}P NMR bands on this attribution [87-90]. Otherwise, several authors working on phosphate adsorption or grafting (involving calcination of the compounds after contact with phosphate solution) on titanium dioxide interpreted their spectra on the basis of this evolution, suggesting thus that ^{31}P chemical shift decreased from monodentate surface complexes to tridentate ones [60, 91, 92]. However, theoretical calculations showed that the chemical shifts of chemisorbed orthophosphates on the surface of TiO_2 is quite different from those determined in bulk titanium phosphates [83]. In that study of Tielens *et al.*, physisorbed phosphates give rise to a ^{31}P NMR band at 4.9 ppm, monodentate complexes to a band at -9.5 ppm, bidentate ones at 2.0 ppm, and tridentate ones at -6.2 ppm. Thus, the trend observed in bulk titanium phosphates seems not to be followed for adsorbed phosphated species at the TiO_2 surface. Even if we excluded the possibility of tridentate species formation in the case of our study, the attribution of the ^{31}P NMR bands we propose is in agreement with that of Tielens *et al*. work, bidentate species presenting a higher chemical shift that monodentate ones, with similar numerical values.

CONCLUSION AND PROSPECTS

The interactions between phosphated compounds and the surface of anatase were examined by infrared and ^{31}P solid-state NMR spectroscopic characterization, coupled with adsorption isotherms and zeta potential measurements. This multi-scale and multi-technique study, proposing an original and systematic investigation process, enabled us to propose possible binding modes of these species on the solid surface of TiO_2. Hence, the main binding mode for phosphates and MEP molecules is undoubtedly bidentate, even if some monodentate species could also be present on the surface, whereas no tridentate complexes formation could be evidenced. DEP is likely to adsorb both through monodentate and bidentate complexes, while TEP is only adsorbed in very few amount, with formation of possible monodentate structures. These assignments were mainly proposed on the basis of NMR results, which revealed discrepancies with previous publications about ^{31}P NMR chemical shifts of adsorbed phosphated compounds on the TiO_2 surface: bidentate species seem to present higher chemical shifts than monodentate ones, in contrast with the ^{31}P chemical shift behavior observed in the bulk titanium phosphates compounds.

This study completes our previous work [28], where we suggested that the hydroxyl groups of either the terminal glycerol unit or the carboxylate unit of phospholipid molecules could be involved in the interaction with the TiO_2 surface. Indeed, as for DEP molecules in this paper, the observed interaction may be due to the formation of bidentate complexes through both free oxygen atoms available on the phosphorus center. Further analyses by spectroscopic methods are needed to confirm this hypothesis. The results presented here also bring a better understanding of the surface state of E171 additive, since this compound is possibly modified with phosphate groups adsorbed or grafted on its surface, as shown by Dudefoi *et al*. [4]. Preliminary ^{31}P NMR results (data not shown) revealed that the chemical environment of phosphorus atoms on the E171 surface

may be similar to that of phosphated species adsorbed on anatase. An accurate analysis of ^{31}P NMR spectra of E171 powders, compared to those obtained in this study, should bring interesting information on the kind of complexes formed on the surface of E171 additives. This would be of key interest in the understanding of the reactivity of these additives in biological environments. Such a study could also be useful to understand how phosphorylated peptides or proteins are specifically retained at the surface of TiO_2 particles in titanium dioxide-based affinity chromatography, and to analyse more finely the mechanisms of retention according to pH and to the molecular structure of the studied compounds.

To complete this study and get more precise information on the kind of complexes really formed between phosphated compounds and the anatase surface, theoretical calculations will be performed, firstly to determine the energetically more favorable binding modes for each phosphated molecule, and secondly to calculate both corresponding IR wavenumbers and ^{31}P NMR chemical shifts. A comparison with the experimental results presented here will enable more accurate assignment of each spectroscopic band to the involved bonds or chemical environments. To reach quantitative data from infrared measurements, we are developing a statistical approach to correlate infrared signals to the amount of phosphated species adsorbed all along the adsorption isotherms. In parallel, performing NMR experiments on higher magnetic field spectrometers, maybe coupled with DNP, would also help us to determine more precisely the chemical environment of phosphorus atoms for each observed band (for example through the evolution of the cross-polarization signal according to the contact time, or by ^{1}H-^{31}P 2D correlations). Experiments of ^{17}O NMR could also be considered, after isotopic enrichment of the compounds. Finally, deuteration experiments for IR measurements could be interesting, both to distinguish better the contributions of P-OH and P=O bonds, which overlap in our spectra, and to evidence the possible presence of hydrogen bonds between the adsorbed phosphated compounds and the anatase surface.

CRediT authorship contribution statement

Florentine GUIOT, Clément PRAUD, and Michaël PARIS: investigation, validation, visualization. **Sophie QUILLARD, Marie-Hélène ROPERS, Bernard HUMBERT, and Hélène TERRISSE:** conceptualization, methodology, investigation, supervision, project administration, and writing.

REFERENCES

[1] S. Farrokhpay, A review of polymeric dispersant stabilisation of titania pigment, Advances in Colloid and Interface Science 151(1-2) (2009) 24-32. DOI: 10.1016/j.cis.2009.07.004.

[2] A. Weir, P. Westerhoff, L. Fabricius, K. Hristovski, N. von Goetz, Titanium Dioxide Nanoparticles in Food and Personal Care Products, Environmental Science & Technology 46(4) (2012) 2242-2250. DOI: 10.1021/es204168d.

[3] W. Dudefoi, H. Terrisse, A.F. Popa, E. Gautron, B. Humbert, M.-H. Ropers, Evaluation of the content of TiO2 nanoparticles in the coatings of chewing gums, Food additives & contaminants. Part A, Chemistry Analysis Control Exposure & Risk Assessment 35(2) (2018) 211-221. DOI: 10.1080/19440049.2017.1384576.

[4] W. Dudefoi, H. Terrisse, M. Richard-Plouet, E. Gautron, F. Popa, B. Humbert, M.-H. Ropers, Criteria to define a more relevant reference sample of titanium dioxide in the context of food: a multiscale approach, Food Additives and Contaminants. Part A, Chemistry Analysis Control Exposure & Risk Assessment 34(5) (2017) 653-665. DOI: 10.1080/19440049.2017.1284346.

[5] R. Peters, G. van Bemmel, Z. Herrera-Rivera, H. Helsper, H. Marvin, S. Weigel, P. Tromp, A. Oomen, A. Rietveld, H. Bouwmeester, Characterization of Titanium Dioxide Nanoparticles in Food Products: Analytical Methods To Define Nanoparticles, Journal of Agricultural and Food Chemistry 62(27) (2014) 6285-6293. DOI: 10.1021/jf5011885.

[6] Y. Yang, K. Doudrick, X. Bi, K. Hristovski, P. Herckes, P. Westerhoff, R. Kaegi, Characterization of Food-Grade Titanium Dioxide: The Presence of Nanosized Particles, Environmental Science & Technology 48(11) (2014) 6391-6400. DOI: 10.1021/es500436x.

[7] E. Verleysen, N. Waegeneers, F. Brassinne, S. De Vos, I. Jimenez, S. Mathioudaki, J. Mast, Physicochemical Characterization of the Pristine E171 Food Additive by Standardized and Validated Methods, Nanomaterials 10(3) (2020) 592. DOI: 10.3390/nano10030592.
[8] J. Lim, D. Bae, A. Fong, Titanium Dioxide in Food Products: Quantitative Analysis Using ICP-MS and Raman Spectroscopy, Journal of Agricultural and Food Chemistry 66(51) (2018) 13533-13540. DOI: 10.1021/acs.jafc.8b06571.
[9] O. Geiss, J. Ponti, C. Senaldi, I. Bianchi, D. Mehn, J. Barrero, D. Gilliland, R. Matissek, E. Anklam, Characterisation of food grade titania with respect to nanoparticle content in pristine additives and in their related food products, Food additives & contaminants. Part A, Chemistry Analysis Control Exposure & Risk Assessment 37(2) (2020) 239-253. DOI: 10.1080/19440049.2019.1695067.
[10] R. Prasad, K. Wallace, K. Daniel, A. Tennant, R. Zucker, J. Strickland, K. Dreher, A. Kligerman, C. Blackman, D. DeMarini, Effect of Treatment Media on the Agglomeration of Titanium Dioxide Nanoparticles: Impact on Genotoxicity, Cellular Interaction, and Cell Cycle, ACS Nano 7(3) (2013) 1929-1942. DOI: 10.1021/nn302280n.
[11] G. Falck, H. Lindberg, S. Suhonen, M. Vippola, E. Vanhala, J. Catalan, K. Savolainen, H. Norppa, Genotoxic effects of nanosized and fine TiO2, Human & Experimental Toxicology 28(6-7) (2009) 339-352. DOI: 10.1177/0960327109105163.
[12] S. Bettini, E. Boutet-Robinet, C. Cartier, C. Comera, E. Gaultier, J. Dupuy, N. Naud, S. Tache, P. Grysan, S. Reguer, N. Thieriet, M. Refregiers, D. Thiaudiere, J. Cravedi, M. Carriere, J. Audinot, F. Pierre, L. Guzylack-Piriou, E. Houdeau, Food-grade TiO2 impairs intestinal and systemic immune homeostasis, initiates preneoplastic lesions and promotes aberrant crypt development in the rat colon, Scientific Reports 7 (2017) 40373. DOI: 10.1038/srep40373.
[13] J. Gurr, A. Wang, C. Chen, K. Jan, Ultrafine titanium dioxide particles in the absence of photoactivation can induce oxidative damage to human bronchial epithelial cells, Toxicology 213(1-2) (2005) 66-73. DOI: 10.1016/j.tox.2005.05.007.
[14] S. Hackenberg, G. Friehs, K. Froelich, C. Ginzkey, C. Koehler, A. Scherzed, M. Burghartz, R. Hagen, N. Kleinsasser, Intracellular distribution, geno- and cytotoxic effects of nanosized titanium dioxide particles in the anatase crystal phase on human nasal mucosa cells, Toxicology Letters 195(1) (2010) 9-14. DOI: 10.1016/j.toxlet.2010.02.022.
[15] S. Kang, Y. Lee, B. Kim, Y. Choi, H. Chung, Cytotoxicity and genotoxicity of titanium dioxide nanoparticles in UVA-irradiated normal peripheral blood lymphocytes, Drug and Chemical Toxicology 34(3) (2011) 277-284. DOI: 10.3109/01480545.2010.546800.
[16] S. Kang, B. Kim, Y. Lee, S. Hong, H. Chung, Titanium dioxide nanoparticles induce apoptosis through the JNK/p38-caspase-8-Bid pathway in phytohemagglutinin-stimulated human lymphocytes, Biochemical and Biophysical Research Communications 386(4) (2009) 682-687. DOI: 10.1016/j.bbrc.2009.06.097.
[17] Q. Rahman, M. Lohani, E. Dopp, H. Pemsel, L. Jonas, D. Weiss, D. Schiffmann, Evidence that ultrafine titanium dioxide induces micronuclei and apoptosis in Syrian hamster embryo fibroblasts, Environmental Health Perspectives 110(8) (2002) 797-800. DOI: 10.1289/ehp.02110797.
[18] J. Wang, C. Chen, Y. Liu, F. Jiao, W. Li, F. Lao, Y. Li, B. Li, C. Ge, G. Zhou, Y. Gao, Y. Zhao, Z. Chai, Potential neurological lesion after nasal instillation of TiO2 nanoparticles in the anatase and rutile crystal phases, Toxicology Letters 183(1-3) (2008) 72-80. DOI: 10.1016/j.toxlet.2008.10.001.
[19] J. Wang, B. Sanderson, H. Wang, Cyto- and genotoxicity of ultrafine TiO2 particles in cultured human lymphoblastoid cells, Mutation Research-Genetic Toxicology and Environmental Mutagenesis 628(2) (2007) 99-106. DOI: 10.1016/j.mrgentox.2006.12.003.
[20] J. Wang, G. Zhou, C. Chen, H. Yu, T. Wang, Y. Ma, G. Jia, Y. Gao, B. Li, J. Sun, Y. Li, F. Jiao, Y. Zhao, Z. Chai, Acute toxicity and biodistribution of different sized titanium dioxide particles in mice after oral administration, Toxicology Letters 168(2) (2007) 176-185. DOI: 10.1016/j.toxlet.2006.12.001.
[21] B. Trouiller, R. Reliene, A. Westbrook, P. Solaimani, R. Schiestl, Titanium Dioxide Nanoparticles Induce DNA Damage and Genetic Instability In vivo in Mice, Cancer Research 69(22) (2009) 8784-8789. DOI: 10.1158/0008-5472.CAN-09-2496.
[22] M. Skocaj, M. Filipic, J. Petkovic, S. Novak, Titanium dioxide in our everyday life; is it safe?, Radiology and Oncology 45(4) (2011) 227-247. DOI: 10.2478/v10019-011-0037-0.
[23] H.B. Shi, R. Magaye, V. Castranova, J.S. Zhao, Titanium dioxide nanoparticles: a review of current toxicological data, Particle and Fibre Toxicology 10 (2013) 33. DOI: 10.1186/1743-8977-10-15.
[24] B. Schanen, A. Karakoti, S. Seal, D. Drake, W. Warren, W. Self, Exposure to Titanium Dioxide Nanomaterials Provokes Inflammation of an in Vitro Human Immune Construct, ACS Nano 3(9) (2009) 2523-2532. DOI: 10.1021/nn900403h.

[25] K. Gerloff, I. Fenoglio, E. Carella, J. Kolling, C. Albrecht, A.W. Boots, I. Foerster, R.P.F. Schins, Distinctive Toxicity of TiO2 Rutile/Anatase Mixed Phase Nanoparticles on Caco-2 Cells, Chemical Research in Toxicology 25(3) (2012) 646-655. DOI: 10.1021/tx200334k.
[26] J. Faust, K. Doudrick, Y. Yang, P. Westerhoff, D. Capco, Food grade titanium dioxide disrupts intestinal brush border microvilli in vitro independent of sedimentation, Cell Biology and Toxicology 30(3) (2014) 169-188. DOI: 10.1007/s10565-014-9278-1.
[27] H. Abdel-Latif, M. Dawood, S. Menanteau-Ledouble, M. El-Matbouli, Environmental transformation of n-TiO2 in the aquatic systems and their ecotoxicity in bivalve mollusks: A systematic review, Ecotoxicology and Environmental Safety 200 (2020) 110776. DOI: 10.1016/j.ecoenv.2020.110776.
[28] Q. Le, M. Ropers, H. Terrisse, B. Humbert, Interactions between phospholipids and titanium dioxide particles, Colloids and Surfaces B-Biointerfaces 123 (2014) 150-157. DOI: 10.1016/j.colsurfb.2014.09.010.
[29] M. Aranha, D. Mukherjee, L. Petridis, B. Khomami, An Atomistic Molecular Dynamics Study of Titanium Dioxide Adhesion to Lipid Bilayers, Langmuir 36(4) (2020) 1043-1052. DOI: 10.1021/acs.langmuir.9b03075.
[30] A. Fortunelli, S. Monti, Simulations of lipid adsorption on TiO2 surfaces in solution, Langmuir 24(18) (2008) 10145-10154. DOI: 10.1021/la801787s.
[31] M. Golub, D. Lott, E. Watkins, V. Garamus, B. Luthringer, M. Stoermer, A. Schreyer, R. Willumeit, X-ray and neutron investigation of self-assembled lipid layers on a titanium surface, Biointerphases 8(21) (2013). DOI: 10.1186/1559-4106-8-21.
[32] E. Guzman, E. Santini, M. Ferrari, L. Liggieri, F. Ravera, Effect of the Incorporation of Nanosized Titanium Dioxide on the Interfacial Properties of 1,2-Dipalmitoyl-sn-glycerol-3-phosphocholine Langmuir Monolayers, Langmuir 33(40) (2017) 10715-10725. DOI: 10.1021/acs.langmuir.7b02484.
[33] J. Jackman, G. Zan, Z. Zhao, N. Cho, Contribution of the Hydration Force to Vesicle Adhesion on Titanium Oxide, Langmuir 30(19) (2014) 5368-5372. DOI: 10.1021/la404581d.
[34] C. Jiang, A. Gamarnik, C. Tripp, Identification of lipid aggregate structures on TiO2 surface using headgroup IR bands, Journal of Physical Chemistry B 109(10) (2005) 4539-4544. DOI: 10.1021/jp046042h.
[35] I. Reviakine, F. Rossetti, A. Morozov, M. Textor, Investigating the properties of supported vesicular layers on titanium dioxide by quartz crystal microbalance with dissipation measurements, Journal of Chemical Physics 122(20) (2005) 204711. DOI: 10.1063/1.1908500.
[36] F. Rossetti, M. Textor, I. Reviakine, Asymmetric distribution of phosphatidyl serine in supported phospholipid bilayers on titanium dioxide, Langmuir 22(8) (2006) 3467-3473. DOI: 10.1021/la053000.
[37] S. Tosatti, R. Michel, M. Textor, N. Spencer, Self-assembled monolayers of dodecyl and hydroxy-dodecyl phosphates on both smooth and rough titanium and titanium oxide surfaces, Langmuir 18(9) (2002) 3537-3548. DOI: 10.1021/la011459p.
[38] F. Wang, J. Liu, A Stable Lipid/TiO2 Interface with Headgroup-Inversed Phosphocholine and a Comparison with SiO2, Journal of the American Chemical Society 137(36) (2015) 11736-11742. DOI: 10.1021/jacs.5b06642.
[39] X. Wang, X. Li, H. Wang, X. Zhang, L. Zhang, F. Wang, J. Liu, Charge and Coordination Directed Liposome Fusion onto SiO2 and TiO2 Nanoparticles, Langmuir 35(5) (2019) 1672-1681. DOI: 10.1021/acs.langmuir.8b02979.
[40] C. Zhang, Y. Liu, S. Wen, J. Luo, Insight into the formation mechanism of durable hexadecylphosphonic acid bilayers on titanium alloy through interfacial analysis, Colloids and Surfaces A-Physicochemical and Engineering Aspects 447 (2014) 51-58. DOI: 10.1016/j.colsurfa.2014.01.056.
[41] P.A. Connor, A.J. McQuillan, Phosphate adsorption onto TiO2 from aqueous solutions: An in situ internal reflection infrared spectroscopic study, Langmuir 15(8) (1999) 2916-2921. DOI: 10.1021/la980894p.
[42] W. Gong, A real time in situ ATR-FTIR spectroscopic study of linear phosphate adsorption on titania surfaces, International Journal of Mineral Processing 63(3) (2001) 147-165. DOI: 10.1016/S0301-7516(01)00045-X.
[43] K. Hadjiivanov, D. Klissurski, A. Davydov, Study of phosphate-modified TiO2 (anatase), Journal of Catalysis 116(2) (1989) 498-505. DOI: 10.1016/0021-9517(89)90116-4.
[44] A.T. Myller, J.J. Karhe, T.T. Pakkanen, Preparation of aminofunctionalized TiO2 surfaces by binding of organophosphates, Applied Surface Science 257(5) (2010) 1616-1622. DOI: 10.1016/j.apsusc.2010.08.109.
[45] D. Zhao, C. Chen, Y. Wang, H. Ji, W. Ma, L. Zang, J. Zhao, Surface modification of TiO2 by phosphate: Effect on photocatalytic activity and mechanism implication, Journal of Physical Chemistry C 112(15) (2008) 5993-6001. DOI: 10.1021/jp712049c.
[46] C. Calvano, O. Jensen, C. Zambonin, Selective extraction of phospholipids from dairy products by micro-solid phase extraction based on titanium dioxide microcolumns followed by MALDI-TOF-MS analysis, Analytical and Bioanalytical Chemistry 394(5) (2009) 1453-1461. DOI: 10.1007/s00216-009-2812-y.
[47] K. Engholm-Keller, M. Larsen, Titanium dioxide as chemo-affinity chromatographic sorbent of biomolecular compounds - Applications in acidic modification-specific proteomics, Journal of Proteomics 75(2) (2011) 317-328.

DOI: 10.1016/j.jprot.2011.07.024.
[48] T. Thingholm, T. Jorgensen, O. Jensen, M. Larsen, Highly selective enrichment of phosphorylated peptides using titanium dioxide, Nature Protocols 1(4) (2006) 1929-1935. DOI: 10.1038/nprot.2006.185.
[49] M. Larsen, T. Thingholm, O. Jensen, P. Roepstorff, T. Jorgensen, Highly selective enrichment of phosphorylated peptides from peptide mixtures using titanium dioxide microcolumns, Molecular & Cellular Proteomics 4(7) (2005) 873-886. DOI: 10.1074/mcp.T500007-MCP200.
[50] A. Leitner, M. Sturm, W. Lindner, Tools for analyzing the phosphoproteome and other phosphorylated biomolecules: A review, Analytica Chimica Acta 703(1) (2011) 19-30. DOI: 10.1016/j.aca.2011.07.012.
[51] Q. Shen, W. Dong, M. Yang, L. Li, H. Cheung, Z. Zhang, Lipidomic fingerprint of Almonds (Prunus dulcis L. cv Nonpareil) using TiO2 nanoparticle based matrix solid-phase dispersion and MALDI-TOF/MS and its potential in geographical origin verification, Journal of Agricultural and Food Chemistry 61(32) (2013) 7739-7748. DOI: 10.1021/jf4016448.
[52] R. Tero, G. Sazaki, T. Ujihara, T. Urisu, Anomalous diffusion in supported lipid bilayers induced by oxide surface nanostructures, Langmuir 27(16) (2011) 9662-9665. DOI: 10.1021/la201474h.
[53] C. Dueymes, C. Pirat, R. Pascal, Facile synthesis of simple mono-alkyl phosphates from phosphoric acid and alcohols, Tetrahedron Letters 49(36) (2008) 5300-5301. DOI: 10.1016/j.tetlet.2008.06.083.
[54] Y. Cao, M. Yu, S. Qi, T. Wang, S. Huang, Z. Ren, S. Yan, S. Hu, M. Xu, CO2 adsorption on anatase TiO2(101) surfaces: a combination of UHV-FTIRS and first-principles studies, Physical Chemistry Chemical Physics 19(46) (2017) 31267-31273. DOI: 10.1039/c7cp05375d.
[55] L. Cueto, G. Hirata, E. Sanchez, Thin-film TiO2 electrode surface characterization upon CO2 reduction processes, Journal of Sol-Gel Science and Technology 37(2) (2006) 105-109. DOI: 10.1007/s10971-006-6427-x.
[56] L. Mino, G. Spoto, A. Ferrari, CO2 capture by TiO2 anatase surfaces: a combined DFT and FTIR study, Journal of Physical Chemistry C 118(43) (2014) 25016-25026. DOI: 10.1021/jp507443k.
[57] S. Mishra, A. Choudhary, S. Roy, B. Nanda, Quantum-mechanical process of carbonate complex formation and large-scale anisotropy in the adsorption energy of CO2 on anatase TiO2 (001) surface, Physical Review Materials 2(11) (2018) 115801. DOI: 10.1103/PhysRevMaterials.2.115801.
[58] U. Tumuluri, J. Howe, W. Mounfield, M. Li, M. Chi, Z. Hood, K. Walton, D. Sholl, S. Dai, Z. Wu, Effect of surface structure of TiO2 nanoparticles on CO2 adsorption and SO2 resistance, ACS Sustainable Chemistry & Engineering 5(10) (2017) 9295-9306. DOI: 10.1021/acssuschemeng.7b02295.
[59] J. Barrows, G. Jameson, M. Pope, Structure of a heteropoly blue – The four-electron reduced beta-12-molybdophosphate anion, Journal of the American Chemical Society 107(6) (1985) 1771-1773. DOI: 10.1021/ja00292a059.
[60] S. Kang, W. Li, H. Lee, B. Phillips, Y. Lee, Phosphate uptake by TiO2: Batch studies and NMR spectroscopic evidence for multisite adsorption, Journal of Colloid and Interface Science 364(2) (2011) 455-461. DOI: 10.1016/j.jcis.2011.07.088.
[61] N. Barrow, J. Bowden, A. Posner, J. Quirk, Describing the effects of electrolyte on adsorption of phosphate by a variable charge surface, Soil Research 18(4) (1980) 395-404. DOI: 10.1071/SR9800395.
[62] B. Nelson, R. Candal, R. Corn, M. Anderson, Control of surface and zeta potentials on nanoporous TiO2 films by potential-determining and specifically adsorbed ions, Langmuir 16(15) (2000) 6094-6101. DOI: 10.1021/la9911584.
[63] Y. Arai, D. Sparks, ATR-FTIR spectroscopic investigation on phosphate adsorption mechanisms at the ferrihydrite-water interface, Journal of Colloid and Interface Science 241(2) (2001) 317-326. DOI: 10.1006/jcis.2001.7773.
[64] R.J. Hunter, R.H. Ottewill, Zeta potential in colloid science : principles and applications, Academic Press, London, 1981.
[65] M. Minella, M. Faga, V. Maurino, C. Minero, E. Pelizzetti, S. Coluccia, G. Martra, Effect of fluorination on the surface properties of titania P25 powder: an FTIR study, Langmuir 26(4) (2010) 2521-2527. DOI: 10.1021/la902807g.
[66] C. Deiana, E. Fois, S. Coluccia, G. Martra, Surface structure of TiO2 P25 nanoparticles: infrared study of hydroxy groups on coordinative defect sites, Journal of Physical Chemistry C 114(49) (2010) 21531-21538. DOI: 10.1021/jp107671k.
[67] M.J.D. Low, P. Ramamurthy, Infrared study of the surface properties of phosphoric acid impregnated silica, The Journal of Physical Chemistry 72(9) (1968) 3161-3167. DOI: 10.1021/j100855a014.
[68] Y. Tan, Y. Liu, L. Grover, Effect of phosphoric acid on the properties of magnesium oxychloride cement as a biomaterial, Cement and Concrete Research 56 (2014) 69-74. DOI: 10.1016/j.cemconres.2013.11.001.
[69] J. Kolmas, D. Marek, W. Kolodziejski, Near-infrared (NIR) spectroscopy of synthetic hydroxyapatites and human dental tissues, Applied Spectroscopy 69(8) (2015) 902-912. DOI: 10.1366/14-07720.

[70] P. Campos, A. Albuquerque, R. Angelica, S. Paz, FTIR spectral signatures of amazon inorganic phosphates: Igneous, weathering, and biogenetic origin, Spectrochimica Acta Part A-Molecular and Biomolecular Spectroscopy 251 (2021) 119476. DOI: 10.1016/j.saa.2021.119476.
[71] T. Ishikawa, M. Wakamura, S. Kondo, Surface characterization of calcium hydroxylapatite by Fourier transform infrared spectroscopy, Langmuir 5(1) (1989) 140-144. DOI: 10.1021/la00085a025.
[72] M. Tejedor-Tejedor, M. Anderson, Protonation of phosphate on the surface of goethite as studied by CIR-FTIR and electrophoretic mobility, Langmuir 6(3) (1990) 602-611. DOI: 10.1021/la00093a015.
[73] P. Connor, A. McQuillan, Phosphate adsorption onto TiO2 from aqueous solutions: An in situ internal reflection infrared spectroscopic study, Langmuir 15(8) (1999) 2916-2921. DOI: 10.1021/la980894p.
[74] B. Wan, Y. Yan, F. Liu, W. Tan, J. He, X. Feng, Surface speciation of myo-inositol hexakisphosphate adsorbed on TiO2 nanoparticles and its impact on their colloidal stability in aqueous suspension: A comparative study with orthophosphate, Science of the Total Environment 544 (2016) 134-142. DOI: 10.1016/j.scitotenv.2015.11.157.
[75] X. Li, L. Yan, W. Zhong, M. Kersten, C. Jing, Competitive arsenate and phosphate adsorption on alpha-FeOOH, LaOOH, and nano-TiO2: Two-dimensional correlation spectroscopy study, Journal of Hazardous Materials 414 (2021). DOI: 10.1016/j.jhazmat.2021.125512.
[76] C. Luengo, M. Brigante, J. Antelo, M. Avena, Kinetics of phosphate adsorption on goethite: Comparing batch adsorption and ATR-IR measurements, Journal of Colloid and Interface Science 300(2) (2006) 511-518. DOI: 10.1016/j.jcis.2006.04.015.
[77] A. C. Chapman, L.E. Thirlwell, Spectra of phosphorus compounds - I the infrared spectra of orthophosphates, Spectrochimica Acta 20(6) (1964) 937-947. DOI: 10.1016/0371-1951(64)80094-1.
[78] L. Daasch, D. Smith, Infrared Spectra of Phosphorus Compounds, Analytical Chemistry 23(6) (1951) 853-868. DOI: 10.1021/ac60054a008.
[79] F.S. Mortimer, Vibrational assignment and rotational isomerism in some simple organic phosphates, Spectrochimica Acta 9(4) (1957) 270-281. DOI: 10.1016/0371-1951(57)80142-8.
[80] K. Taga, K. Miyagai, N. Hirabayashi, T. Yoshida, H. Okabayashi, Vibrational-spectra and normal coordinate analysis of barium dimethyl, diethyl and ethyl methyl phosphates, Journal of Molecular Structure 245(1-2) (1991) 1-11. DOI: 10.1016/0022-2860(91)87001-X.
[81] V. Ramakrishnan, G. Aruldhas, Vibrational studies of two phosphotellurates: Te(OH)62(NH4)2HPO4 and Te(OH)6Na2HPO4· H2O, Infrared Physics 26(5) (1986) 293-297. DOI: 10.1016/0020-0891(86)90006-0.
[82] E. Espinosa, B. Wyncke, F. Brehat, X. Gerbaux, S. Veintemillas, E. Molins, Infrared vibrational spectra of L-histidinium dihydrogen orthophosphate orthophosphoric acid (LHP), Infrared Physics & Technology 38(7) (1997) 449-458. DOI: 10.1016/S1350-4495(97)00029-7.
[83] F. Tielens, C. Gervais, G. Deroy, M. Jaber, L. Stievano, C. Diogo, J. Lambert, Characterization of Phosphate Species on Hydrated Anatase TiO2 Surfaces, Langmuir 32(4) (2016) 997-1008. DOI: 10.1021/acs.langmuir.5b03519.
[84] F. Soria, C. Di Valentin, Binding group of oligonucleotides on TiO2 surfaces: Phosphate anions or nucleobases?, Applied Surface Science 575 (2022) 151560. DOI: 10.1016/j.apsusc.2021.151560.
[85] A. Myller, J. Karhe, T. Pakkanen, Preparation of aminofunctionalized TiO2 surfaces by binding of organophosphates, Applied Surface Science 257(5) (2010) 1616-1622. DOI: 10.1016/j.apsusc.2010.08.109.
[86] C. Schmutz, P. Barboux, F. Ribot, F. Taulelle, M. Verdaguer, C. Fernandez-Lorenzo, EXAFS, Raman and P-31 NMR-study of amorphous titanium phosphates, Journal of Non-Crystalline Solids 170(3) (1994) 250-262. DOI: 10.1016/0022-3093(94)90054-X.
[87] H. Fei, X. Zhou, H. Zhou, Z. Shen, P. Sun, Z. Yuan, T. Chen, Facile template-free synthesis of meso-macroporous titanium phosphate with hierarchical pore structure, Microporous and Mesoporous Materials 100(1-3) (2007) 139-145. DOI: 10.1016/j.micromeso.2006.10.019.
[88] M. Maslova, D. Rusanova, V. Naydenov, O. Antzutkin, L. Gerasimova, Extended study on the synthesis of amorphous titanium phosphates with tailored sorption properties, Journal of Non-Crystalline Solids 358(22) (2012) 2943-2950. DOI: 10.1016/j.jnoncrysol.2012.06.033.
[89] T. Ren, Z. Yuan, A. Azioune, J. Pireaux, B. Su, Tailoring the porous hierarchy of titanium phosphates, Langmuir 22(8) (2006) 3886-3894. DOI: 10.1021/la0533011.
[90] H. Takahashi, T. Oi, M. Hosoe, Characterization of semicrystalline titanium(IV) phosphates and their selectivity of cations and lithium isotopes, Journal of Materials Chemistry 12(8) (2002) 2513-2518. DOI: 10.1039/b203266j.
[91] T. Kovalchuk, H. Sflhi, A. Korchev, A. Kovalenko, V. Il'in, V. Zaitsev, J. Fraissard, Synthesis, structure, and acidic properties of MCM-41 functionalized with phosphate and titanium phosphate groups, Journal of Physical Chemistry B 109(29) (2005) 13948-13956. DOI: 10.1021/jp0580625.

[92] K. Elghniji, M. Saad, M. Araissi, E. Elaloui, Y. Moussaoui, Chemical modification of TiO2 by H2PO4-/HPO42- anions using the sol-gel route with controlled precipitation and hydrolysis: enhancing thermal stability, Materials Science-Poland 32(4) (2014) 617-625. DOI: 10.2478/s13536-014-0237-6.

FIGURE CAPTIONS

Figure 1: Chemical formulation of phosphated compounds used in the present study. "P" was purchased as the Na_2HPO_4 salt, "MEP" was synthesized under the $[CyNH_3](EtO)PO_3H]$ compound (Cy = cyclohexyl; Et = ethyl), and "DEP" was purchased as the $[EMIM\text{-}(EtO)_2PO_2]$ salt (EMIM = 1-ethyl-3-methylimidazolium).

Figure 2: Adsorption isotherms of phosphates for different pH values at an ionic strength of 0.01 mol/L (fixed with NaCl salt), obtained at 25°C. These data were recorded with 11.5 m^2 of TiO_2 (150 mg of solid with a specific surface area of 76.8 m^2/g) in 40 mL of aqueous solution. The lines have been added as a guide for the eye.

Figure 3: Adsorption isotherms of phosphates at pH 2 for two ionic strengths fixed with NaCl, 0.1 and 0.01 mol/L, at 25°C. These data were recorded with 11.5 m^2 of TiO_2 in 40 mL of aqueous solution. Data at an ionic strength of 0.01 mol/L correspond to Figure 2.

Figure 4: Adsorption isotherms of MEP for different pH values at an ionic strength of 0.01 mol/L (fixed with NaCl salt), at 25°C. These data were recorded with 11.5 m^2 of TiO_2 in 40 mL of aqueous solution.

Figure 5: Adsorption isotherms of MEP, DEP and P at pH 2, for an ionic strength of 0.01 mol/L (fixed with NaCl salt) at 25°C. These data were recorded with 11.5 m^2 of TiO_2 in 40 mL of aqueous solution.

Figure 6: Evolution of zeta potential versus pH for PC100 in contact with phosphate ions at two concentrations 2.5 10^{-6} and 1.0 10^{-5} mol/L), compared with PC100 alone, at a constant ionic strength (0.01 mol/L fixed with NaCl salt). The solid concentration is 0.14 g/L. The lines have been added as a guide for the eye.

Figure 7: Comparative zeta potential versus pH evolution, for PC100 alone and in contact with phosphate ions (P) and substituted phosphate molecules (MEP, DEP, TEP) at the same concentration ($[P] = 10^{-5}$ mol/L), with a constant ionic strength fixed with NaCl (0.01 mol/L). The solid concentration is 0.14 g/L. The lines have been added as a guide for the eye.

Figure 8: DRIFTS spectra of PC100 powder after adsorption of phosphated species, at pH 2 and with an ionic strength of 0.01 mol/L: A) 5000-2500 cm^{-1}; B) 3800-3500 cm^{-1}; C) Near infrared range, 4750-4500 cm^{-1}.
a) reference PC100; b) TEP_{ads}; c) DEP_{ads}; d) MEP_{ads}; e) P_{ads} (the spectra are offset for visibility, and the combination modes involving P-O-H are evidenced by band coloring).

Figure 9: MIR-ATR spectra of PC100 after adsorption of phosphated molecules, at pH 2 and with an ionic strength of 0.01 mol/L: A) as-recorded spectra; B) spectra after subtraction of the PC100 surface reference.
a) reference PC100; b) TEP_{ads}; c) DEP_{ads}; d) MEP_{ads}; e) P_{ads} (the spectra are offset for visibility; the as-recorded spectra are not labelled to avoid the perturbation coming from the strong absorption of TiO_2).

Figure 10: A and B) DRIFTS and C and D) MIR-ATR spectra of PC100 after adsorption of non-substituted phosphate ions with an ionic strength of 0.01 mol/L (C: as-recorded spectra, D: spectra after subtraction of the reference PC100 at the same pH).
a) pH 2, b) pH 6, c) pH 9 (the as-recorded spectra are not labelled to avoid the perturbation coming from the strong absorption of TiO_2).

Figure 11: NIR-DRIFTS (4500-4750 cm^{-1}) and MIR-ATR (850-1500 cm^{-1}) spectra of PC100 after adsorption of phosphated molecules, with an ionic strength of 0.01 mol/L; A and B) pH 6; C and D) pH 9.
a) Reference PC100; b) TEP_{ads}; c) DEP_{ads}; d) MEP_{ads}; e) P_{ads}.

Figure 12: $\{^1H\}$-^{31}P CP-MAS NMR spectra of PC100 after adsorption of phosphated molecules, at pH 2 and with an ionic strength of 0.01 mol/L.

Figure 13: {^{1}H}-^{31}P CP-MAS NMR spectra of PC100 after adsorption of phosphate ions, for various pH values (2, 6 and 9), with an ionic strength of 0.01 mol/L.

Figure 14: {^{1}H}-^{31}P CP-MAS NMR spectra of PC100 after adsorption of phosphated molecules at pH 6 (A) and pH 9 (B), for an ionic strength of 0.01 mol/L.

Figure 15: Propositions of binding modes for the various phosphated molecules on anatase surface. For simplification, water molecules are not included in these schemes.

TABLES

Table 1: Main characteristics of phosphated molecules adsorption at the PC100 anatase surface, including maximum adsorbed amount at three pH values, IEP of PC100 in the presence of phosphated molecules for [P] = 10^{-5} mol/L, main infrared bands with their qualitative intensities and their attributions, estimated relative adsorbed amounts at pH 2 extracted from IR spectra, and ^{31}P NMR chemical shifts with their proposed assignment. IR and NMR data are only given at pH 2, where the adsorbed amount reaches its maximum for each phosphated molecule. Band intensity is categorized as (+) low, (++) medium and (+++) high.

SUPPLEMENTARY MATERIAL

1/ Characterization of anatase particles

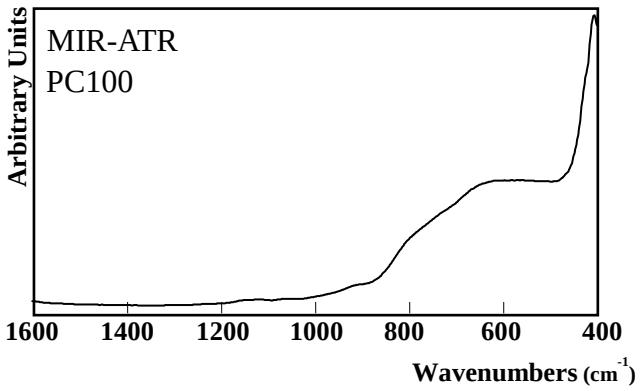

Figure S1: ATR spectra of PC100 power, showing no band in the region of nitrate signature (around 1300 cm^{-1}).

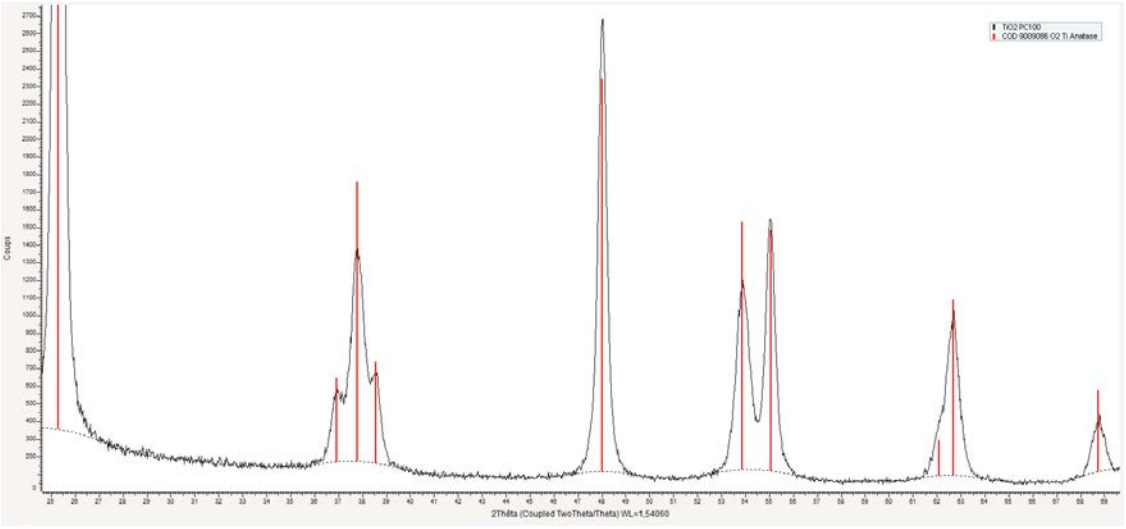

Figure S2: X-ray diagram of PC100 power, showing that it is composed of anatase only.

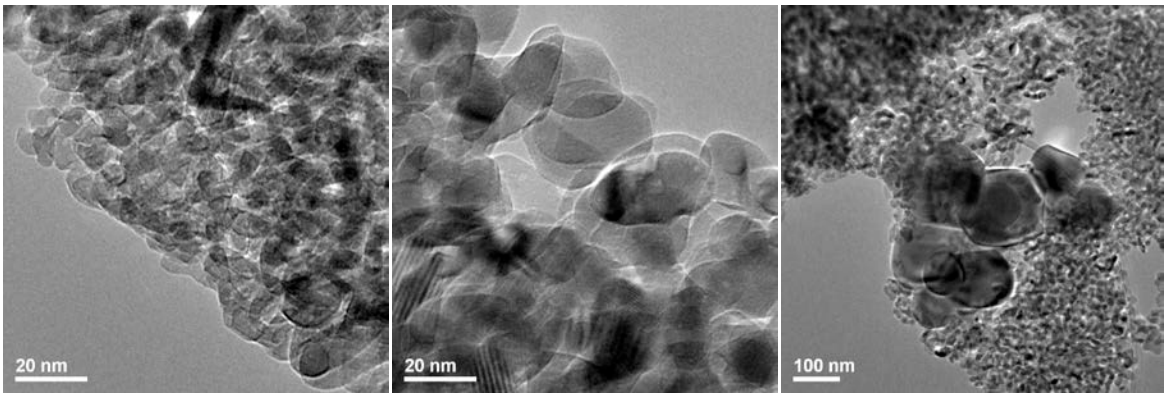

Figure S3: TEM images of PC100 particles.

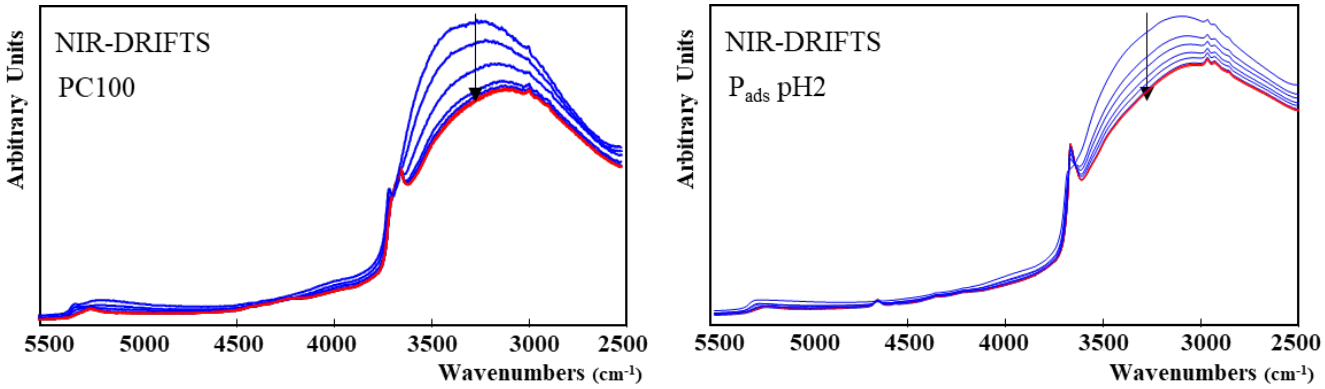

Figure S4: NIR-DRIFTS spectra upon dehydration during 3 hours (examples of pristine PC100 at left, and PC100 with adsorbed P at pH 2 at right). The arrow indicates the evolution in time. Blue spectra are at the beginning, red ones at the end of the 3 hours. Spectra were taken every 10 minutes.

2/ NMR characterization of DEP and TEP adsorption on PC100 surface

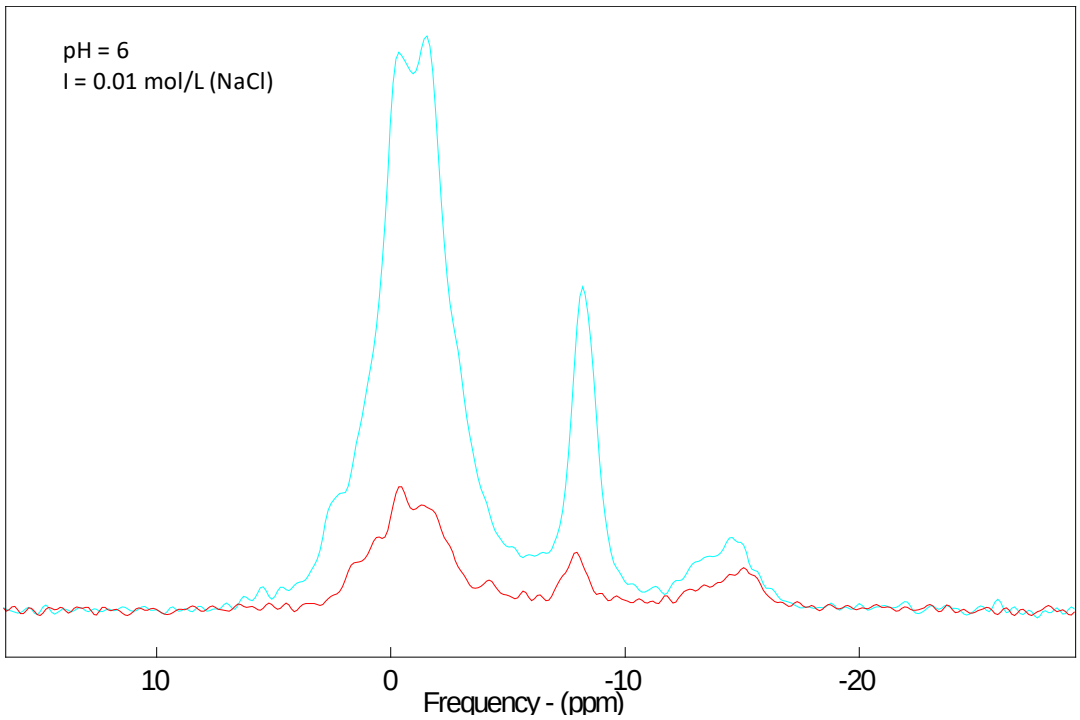

Figure S5: {^{1}H}-^{31}P CP-MAS NMR spectra of PC100 in contact with DEP and TEP at pH 6 and with an ionic strength of 0.01 mol/L, for two acquisition times (24 hours in blue against 6 hours in red).